

# The VMC Survey - VI. Quasars behind the Magellanic system<sup>★</sup>

M.-R.L. Cioni<sup>1,2,★★</sup>, D. Kamath<sup>3</sup>, S. Rubele<sup>4</sup>, J.Th. van Loon<sup>5</sup>, P.R. Wood<sup>3</sup>, J.P. Emerson<sup>6</sup>, B. K. Gibson<sup>7</sup>, M.A.T. Groenewegen<sup>8</sup>, V.D. Ivanov<sup>9</sup>, B. Miszalski<sup>10,11</sup>, and V. Ripepi<sup>12</sup>

<sup>1</sup> University Observatory Munich, Scheinerstrasse 1, 81679 München, Germany

<sup>2</sup> University of Hertfordshire, Physics Astronomy and Mathematics, Hatfield AL10 9AB, United Kingdom

<sup>3</sup> Research School of Astronomy and Astrophysics, Mount Stromlo Observatory, Cotter Road, Weston Creek, ACT 2611, Australia

<sup>4</sup> INAF, Osservatorio Astronomico di Padova, Vicolo dell'Osservatorio 5, 35122 Padova, Italy

<sup>5</sup> Keele University, Lennard-Jones Laboratories, ST5 5BG, United Kingdom

<sup>6</sup> School of Physics and Astronomy, Queen Mary University of London, Mile End Road, London E1 4NS, United Kingdom

<sup>7</sup> Jeremiah Horrocks Institute, University of Central Lancashire, Preston PR1 2HE, United Kingdom

<sup>8</sup> Royal Observatory of Belgium, Ringlaan 3, 1180 Ukkel, Belgium

<sup>9</sup> European Southern Observatory, Av. Alonso de Córdoba 3107, Casilla 19, Santiago, Chile

<sup>10</sup> South African Astronomical Observatory, PO Box 9, Observatory, 7935, South Africa

<sup>11</sup> Southern African Large Telescope Foundation, PO Box 9, Observatory, 7935, South Africa

<sup>12</sup> INAF, Osservatorio Astronomico di Capodimonte, via Moirariello 16, 80131 Napoli, Italy

Received 28 May 2012 / Accepted

## ABSTRACT

**Context.** The number and spatial distribution of confirmed quasi-stellar objects (QSOs) behind the Magellanic system is limited. This undermines their use as astrometric reference objects for studies of proper motion and of the interstellar medium along the line of sight.

**Aims.** We search for criteria to identify candidate QSOs using near-infrared observations from the VISTA survey of the Magellanic Clouds system (VMC). The VMC survey provides photometry in the  $YJK_s$  bands and 12 epochs in the  $K_s$  band with unprecedented sensitivity and spatial resolution.

**Methods.** The  $(Y - J)$  versus  $(J - K_s)$  diagram has been used to distinguish QSO candidates from Milky Way stars and stars of the Magellanic Clouds. Then, the slope of variation in the  $K_s$  band has been used to identify a sample of high confidence candidates. These criteria were developed based on the properties of 117 known QSOs presently observed by the VMC survey where the  $K_s$  epochs span a time range up to 600 days.

**Results.**  $YJK_s$  magnitudes and  $K_s$  light-curves of known QSOs behind the Magellanic system from present VMC data are presented. About 75% of them show a slope of variation  $> 10^{-4}$  mag/day and the shape of the light-curve is in general irregular and without any clear periodicity. A method to identify QSOs based solely on the VMC data is proposed using  $YJK_s$  colours and  $K_s$  variability. The number of QSO candidates found in tiles including the South Ecliptic Pole and the 30 Doradus regions is 22 and 26, respectively, with negligible contamination by young stellar objects, planetary nebulae, stars and normal galaxies. The high confidence in the nature of the selected objects is supported by recent studies of possible contaminants, but remains to be confirmed by spectroscopic follow up.

**Conclusions.** By extrapolating the number of QSO candidates to the entire VMC survey area we expect to find about 1500 QSOs behind the LMC, 600 behind the SMC, 300 behind the Bridge and 50 behind the Stream areas. Without magnitude restrictions and allowing for de-blended objects, the VMC survey can find candidates  $> 1$  mag fainter than those presented in this work. The VMC survey has the potential to reveal the remaining 85% of the QSOs behind the Magellanic system. Further, the  $K_s$  light-curves can help support investigations of the mechanism responsible for the variations. The confirmed QSOs found from these candidates will provide a good astrometric reference grid for proper motion studies of the Magellanic system.

**Key words.** Surveys - Magellanic Clouds - quasars: general - Infrared: galaxies

## 1. Introduction

The astrometric accuracy and the photometric sensitivity of observations made with VISTA is sufficiently good that we expect data from the VISTA Magellanic Clouds survey (VMC; PI Cioni; Cioni et al. 2011 hereafter Paper I) can be used

to derive proper motions of the Magellanic Clouds (MCs). Such proper motion studies require a reference grid of bright, distant, non-moving, point like objects. Quasi-stellar objects (QSOs) provide such a grid (e.g. Kallivayalil et al. 2006; Costa et al. 2011). QSOs are point-like sources believed to be powered by accretion onto black holes in the centre of distant galaxies. Besides being reliable astrometric reference objects for studies of proper motion, they can also be used as background sources to examine the composition of the MC interstellar medium along the line of sight (e.g. Redfield et al. 2006;

Send offprint requests to: mcioni@usm.uni-muenchen.de

<sup>★</sup> Based on observations made with VISTA at the Paranal Observatory under program ID 179.B-2003.

<sup>★★</sup> Research Fellow of the Alexander von Humboldt Foundation

van Loon et al. 2009), and are important for studies of galaxy formation and evolution.

The density of QSOs with  $i < 19$  mag is  $\sim 11$  per  $\text{deg}^2$  as estimated from the Sloan Digital Sky Survey (SDSS) Quasar Catalogue (Schneider et al. 2010) but discovery of candidate QSOs behind the MCs is complicated by the necessity to distinguish candidate QSOs from the dense stellar content of the MCs themselves. Candidate QSOs must then be observed spectroscopically to confirm which are true QSOs, and to make this process efficient the sample of candidate QSOs should be as clean as possible. Selection of candidate QSOs behind the MCs has been greatly improved by long-term multi-epoch observations, as part of micro-lensing projects such as the MAssive Compact Halo Objects (MACHO – Alcock et al. 2000) and the Optical Gravitational Lensing Experiment (OGLE – Udalski et al. 1992), and using data at various wavelengths, from ultraviolet (UV) to infrared (IR), that permit better removal of stellar objects (young stellar objects, planetary nebulae, hot and red stars) from QSO candidate samples. Methods used to identifying candidate QSOs include X-ray (Shanks et al. 1991) or radio emission (Schmidt 1968), mid-IR (Stern et al. 2005) and near-IR colours (see below). Also flux variations probably associated with the accretion disc have been used (Hook et al. 1994). QSO candidates are spectroscopically confirmed on the basis of optical and UV ionic emission lines, from which their redshifts are measured (e.g. Vanden Berk et al. 2001). The most recent such investigation by Kozłowski et al. (2012) focused on the southern edge of the Large Magellanic Cloud (LMC) and is relatively complete for objects with  $I < 19.2$  mag, with a candidate sample based on Spitzer Space Telescope mid-IR colours, X-ray emission and/or optical variability. Spectra of their sample quadrupled the number of confirmed QSOs behind the LMC.

Currently there are 360 known QSOs behind the Magellanic system of which 233 are behind the LMC, 100 behind the Small Magellanic Cloud (SMC) and 27 behind the inter-cloud region including the Magellanic Bridge, and many more QSO candidates awaiting follow-up observations to establish their nature (e.g. Kozłowski & Kochanek 2009; Kim et al. 2012). However these objects cover a limited area compared to the extent of the whole MC system being surveyed in the VMC survey which covers a wide area around each galaxy, including the Bridge region and a few fields in the Magellanic Stream. VMC detects sources as faint as  $K_s = 23.4$  mag (AB) with  $S/N = 5$ , corresponding to the luminosity of sources below the oldest turn off point of main sequence stars in the LMC which occurs at  $I \sim 22$  mag. The  $YJK_s$  VMC survey, which is multi-epoch in  $K_s$ , has the potential to considerably enlarge the parameter space for the search of QSOs, behind the Magellanic system, both in terms of sensitivity and spatial distribution. Near-IR criteria have been used to select high- $z$  QSOs using data from the UKIRT Infrared Deep Sky Survey (UKIDSS) and SDSS data (Mortlock et al. 2012), and the highest redshift quasar currently known ( $z = 7.085$ , Mortlock et al. 2011) was found, whilst Findlay et al. (2012) used criteria based on single epoch VISTA  $ZYJ$  data to select high redshift ( $6.5 < z < 7.5$ ) QSOs. Kouzuma & Yamaoka (2010) proposed selection of candidate QSOs based on 2MASS  $JHK$  bands, and a series of papers have described the  $K$  excess ( $KX$ ) method using UKIDSS  $JK$  bands and SDSS  $Vg$  bands (Warren, Hewett & Foltz 2000; Maddox et al. 2012).

Our aim is to establish VMC  $YJK_s$  bands selection criteria using the known QSOs behind the Magellanic system which have already been observed (by VMC), and investigate their utility in identifying new candidate QSOs in the areas being surveyed. For our purposes low redshifts are as good as high so the sophistication of the techniques for finding high- $z$  QSOs is not needed. The first stage of the method adopted for VMC regions uses the  $(Y - J)$  vs  $(J - K_s)$  diagram and the second stage uses  $K_s$  variability.

Section 2 describes the known QSO population behind the Magellanic system, and the VMC data acquired up to end of September 2011, before presenting the VMC photometry of those QSOs that have been covered so far. Section 3 uses VMCs  $YJK_s$  photometry of these QSOs to establish colour criteria for isolating them from Milky Way (MW) and MC objects, and to examine the  $K_s$  variability of the QSOs over a baseline of up to 12 epochs over two years. Section 4 discusses how the combination of colour and variability criteria perform on selecting out non-QSOs, using catalogues of various types of objects towards the MCs. Section 5 presents our conclusions on the potential of the  $YJK_s$  photometry and  $K_s$  variability QSO selection method, and the Appendix provides the present sample of VMC  $K_s$  band light-curves of known QSOs.

## 2. Data and Sample

### 2.1. VMC data

The near-IR data analysed in this study were obtained with the Visual and Infrared Survey Telescope for Astronomy (VISTA; Emerson & Sutherland 2010) for the VMC survey and include observations acquired until the end of September 2011. The data were reduced onto the VISTA photometric system (Vegamag = 0) with the VISTA Data Flow System (VDFS) pipeline v1.1 (Irwin et al. 2004) and extracted from the VISTA Science Archive<sup>1</sup> (VSA) using data release VMCv20120126. The VMC survey strategy involves repeated observations of tiles across the Magellanic system, where one tile homogeneously covers an area of  $1.5 \text{ deg}^2$  with 3 epochs in both  $Y$  and  $J$  filters, and 12 epochs in  $K_s$  with the epochs spread over a time range of a year or longer. Details about the observing strategy and the data reduction are given in Paper I.

Table 1 lists the tiles which contain known QSOs and whose observations were by end of September 2011. Tile names are specified in column 1 and the limiting magnitude corresponding to sources with photometric errors  $< 0.1$  mag in columns 2 – 4 while the number of available  $K_s$  epochs is given in column 5 (see also Sect. 3.4).

VMC sources have numerical quality flags and in the following analysis we discriminate sources that are well detected (photometric flag A - with quality flags = 0 – 16 where 16 indicates that a source has been de-blended in at least one wave band), and those with a low quality detection (photometric flag B - with quality flags  $> 16$  that would arise if a source is located in the under-exposed edge areas of a tile, or in the upper half of VISTA's detector #16 which is known to have a varying quantum efficiency, that may result in bad flat fielding and unreliable magnitudes, or just a low confidence in the aperture magnitude of sources). See Paper I for details.

<sup>1</sup> <http://horus.roe.ac.uk/login.html>

**Table 1.** VMC tile sensitivity and epochs.

Tile	Limiting Magnitude <sup>a</sup>			Epochs $K_s$
	$Y$ (mag)	$J$ (mag)	$K_s$ (mag)	
SMC 3_3	20.659	20.412	19.607	9
SMC 3_5	21.127	21.002	19.693	10
SMC 4_3	20.152	19.977	19.071	3
SMC 5_4	20.678	20.461	19.621	11
BRI 2_3	21.222	20.952	19.734	9
BRI 3_7	20.972	20.742	18.418	1
LMC 4_2	21.305	20.593	19.501	8
LMC 4_6	20.652	20.378	18.587	2
LMC 5_5	19.890	19.626	19.081	10
LMC 6_4	19.259	18.962	18.576	10
LMC 6_6 <sup>b</sup>	19.906	19.514	18.995	14
LMC 6_8	20.782	20.585	17.911	1
LMC 7_3	20.406	19.949	18.802	2
LMC 8_3	20.882	20.364	19.676	12
LMC 8_8 <sup>b</sup>	21.091	20.760	19.856	14
LMC 9_7	20.989	20.414	18.226	1

<sup>a</sup> For sources with photometric error < 0.1 mag.<sup>b</sup> VMC observations are completed.

## 2.2. Known quasars

The spatial distribution of the 360 spectroscopically confirmed QSOs behind the Magellanic system is shown in Fig. 1. Most of them, confirmed prior to July 2009, are included in the compilation by Véron-Cetty & Véron (2010) and we use their coordinates, corrected according to Flesch (2012), instead of those from the original studies. The lists of QSOs behind the LMC and SMC are discussed in Sects. 2.2.1 and 2.2.2 below, respectively. For the presently studied VMC dataset only 117 quasars are included within the regions observed by the VMC survey, with most of them contained in tiles LMC 5\_5, LMC 6\_4, SMC 4\_3 and SMC 5\_4 (see Tab. 1 for the sensitivity limits). Tile numbering begins from the bottom right corner, increasing from right to left and from bottom to top. The first LMC tile is 2\_3, the first SMC tile is 2\_2, the first Bridge tile is 1\_2 and Stream tile 1\_1 is right above the Bridge while 2\_1 is to the right of the SMC. The central coordinates of VMC tiles are given in Paper I while the contour plots showing the outer structure and bar of the galaxies as well as the distribution of evolved giant stars are described in Cioni, Habing & Israel (2000).

Figure 1 shows that the distribution of known QSOs is inhomogeneous and biased to the central region of the galaxies. This is because most QSOs were extracted from micro-lensing surveys that have focused their observations on the densest regions, i.e. the bar of the galaxies. In addition, not all candidates from these searches have been spectroscopically observed, further biasing the distribution of confirmed sources.

### 2.2.1. LMC

The list of 233 spectroscopically confirmed quasars behind the LMC comprises 75 QSOs from the Véron-Cetty & Véron (2010) compilation among which 10 were identified as X-ray sources with the Chandra X-ray Observatory satellite and

3 as a result of mining OGLE-II light-curves (Dobrzycki et al. 2002, 2005) while 38 refer to variability in the MACHO database (Geha et al. 2003). In addition, two QSOs used by Anguita et al. (2000) and one by Pedreros et al. (2002) to study the proper motion of the LMC are attributed to a private communication by J. Maza in 1989 and/or do not appear in previous studies. More recently, 1 QSO was confirmed by Hony et al. (2011) and 145 QSOs by Kozłowski et al. (2012), the latter identified from OGLE-III light-curves. The entire MACHO database, with light-curves spanning a time range of  $\sim 7.5$  yr, was searched by Kim et al. (2011, 2012) who trained a support vector machine model with diagnostic features based on mid-IR colours, spectral energy distribution red-shifts and X-ray luminosity of previously known QSOs to identify 663 high confidence candidates, but none of them are at present spectroscopically confirmed. Finally, as part of a spectroscopic study on post asymptotic giant branch (AGB) stars, Kamath et al. (in prep.) confirmed 6 QSOs and detected one broad emission line in 3 additional objects that may also be QSOs.

### 2.2.2. SMC

The list of 100 spectroscopically confirmed quasars behind the SMC comprises 41 QSOs from the Véron-Cetty & Véron (2010) compilation among which 16 were discovered as counterparts to X-ray sources (Tinney, Da Costa & Zinnecker 1997; Tinney 1999; Dobrzycki et al. 2003b), 3 were identified from their OGLE-II light-curves (Eyer 2002; Dobrzycki et al. 2003a) and 9 from their MACHO light-curves (Geha et al. 2003). More recently, Kozłowski et al. (2011) inspected mid-IR colours from the Spitzer Space Telescope and the OGLE-II light-curves of sources in the central  $1.5 \text{ deg}^2$  of the SMC. They confirmed 29 QSOs and showed broad emission lines, typical of QSOs, in 12 additional objects but the signal to noise ratio (S/N) in their spectra was of lower quality. The newest QSOs are from Kamath et al. (in prep.) where 17 are confirmed and 1 is a likely candidate since only one typical QSO broad emission line was detected in its spectrum.

## 2.3. Cross-correlation

VMC detections of the 126 known (spectroscopically confirmed) QSOs covered by VMC data up to September 2011 were selected by searching for the nearest counterpart within  $2''$ . This query to the VSA produced 117 matches in the merged catalogue ("vmcsource") containing  $Y$ ,  $J$  and  $K_s$  band sources extracted from "tiledeepstacks" which are deep tile images resulting from the combination of individual tile images taken at different observing epochs. A further 8 QSOs were matched in the un-merged catalogue, and only one known QSO was undetected. We inspected the images of all 126 objects and most were good and well matched, and we discuss all the matches in Sect. 2.3.1.

### 2.3.1. VMC-QSO distances

Forty QSOs in the LMC from the list by Kozłowski et al. (2012) have counterparts at a mean distance of  $0.33 \pm 0.17''$ . Five matches were rejected because the corresponding VMC source, contrary to the distribution of most counterparts, was found at a distance  $> 1''$  and in all five cases inspection

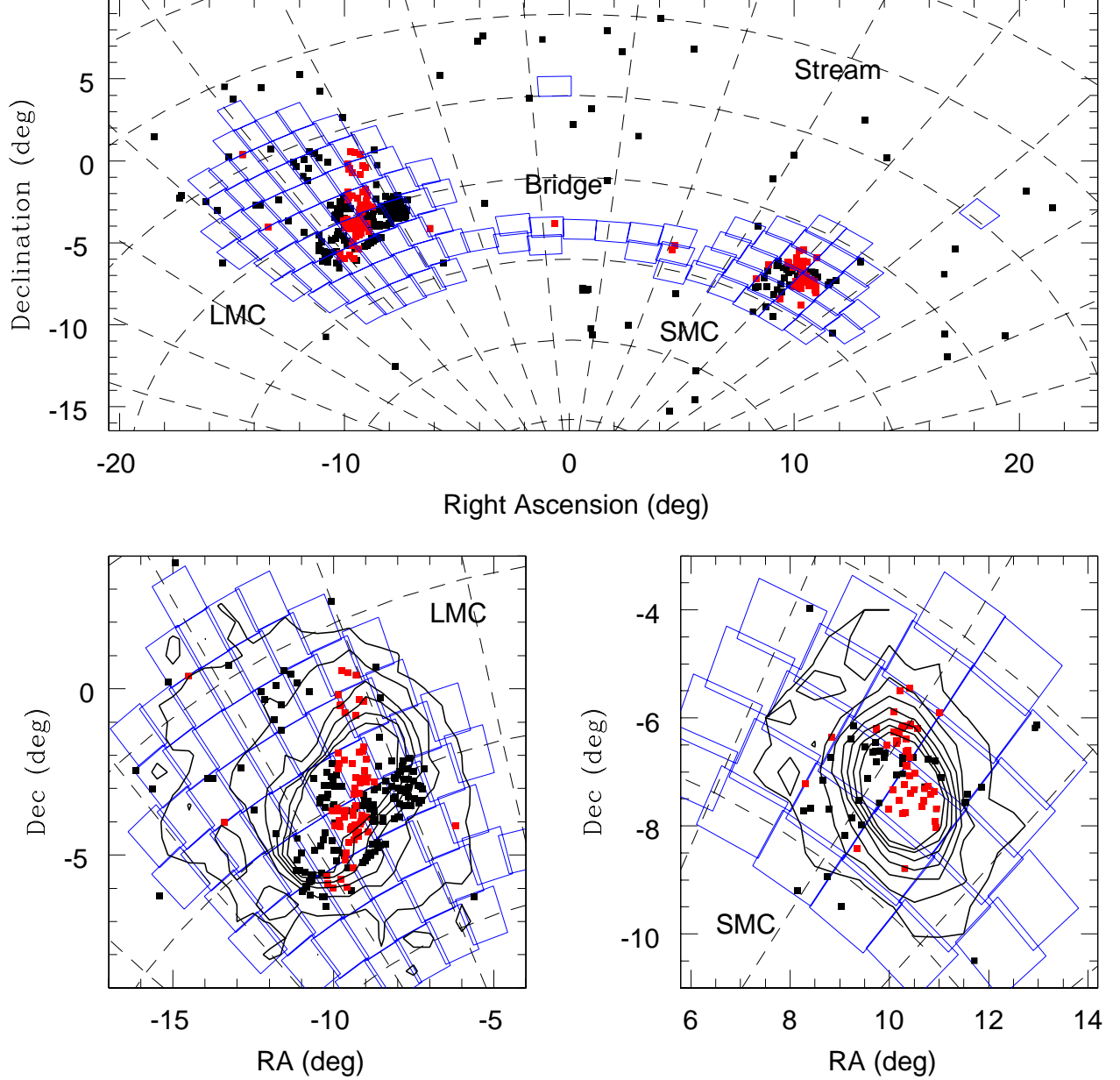


**Fig. 1.** Distribution of known quasars behind the Magellanic system (top) with enlargements on the LMC (bottom-left) and SMC (bottom-right). All known quasars are shown with filled small black squares while those positionally matched with presently available VMC data are shown in red. Large empty blue rectangles indicate the VMC tiles. Contour plots show the distribution of evolved giant stars which delineate the outer structure and bar of the galaxies. Coordinates are given with respect to  $(\alpha_0, \delta_0) = (51^\circ, -69^\circ)$ .

of the VMC images showed another, fainter, object with the typical red colour of QSOs present but not found in the list of nearby objects. A cross-correlation with the “vmcdetection” un-merged catalogue shows that the likely counterparts are indeed located at distances  $\leq 1''$  (Table 3). The counterparts to Kamath et al.’s sources lie at a similar distance, i.e.  $0.31 \pm 0.17''$ .

Seventeen QSOs were matched with the sample by Dobrzycki et al. (2002, 2003a, 2003b, 2005) of which 7 in the SMC and 10 in the LMC. Thirty SMC QSOs were matched from the lists of Kozłowski et al. (2011); 20 from their confirmed list and 10 from their plausible list. Three matches were rejected because their detection in  $Y$  and  $J$  is suspicious; they are faint and close to a brighter object, and their suggested counterparts are at a distance  $> 1.3''$  on average. The likely

counterparts to these QSOs were found in the un-merged catalogue (Table 3). The VMC counterpart to QSOs J004818.76-732059.6, J004831.50-732339.9, J010057.77-722230.8 and J010137.52-720418.9 at  $\sim 1''$  are perhaps affected by the extended nature of the source since all other counterparts lie at smaller distances. Four QSOs were matched with the compilation by Véron-Cetty & Véron (2010) of which 3 in the Bridge and 1 in the LMC; the latter, RXS J05466–6415, is the brightest near-IR quasar in the sample with  $K_s = 13.590 \pm 0.004$  mag. These QSOs were originally confirmed by Perlman et al. (1998) and Healey et al. (2008) for the Bridge and LMC, respectively.

The mean distance of VMC counterparts for quasars from Dobrzycki et al. (2002, 2003a, 2003b, 2005), Kozłowski et al. (2011) and Véron-Cetty & Véron (2010) are very similar and correspond to  $0.64 \pm 0.30''$ . The larger distance of VMC counterparts to the quasars from Kozłowski et al. (2011) compared to the quasars from Kozłowski et al. (2012) is most likely due to their identification from the OGLE database part II in one case and part III in the other. OGLE-II data were obtained with a CCD camera with a scale of  $0.4''/\text{pixel}$  while OGLE-III data were obtained with a new camera with a scale of  $0.26''/\text{pixel}$  and this may introduce a systematic offset in the world-coordinates between the two systems. Both OGLE surveys are well-matched to the VISTA camera which has a scale of  $0.34''/\text{pixel}$ .

Finally, from the list of Geha et al. (2003) 16 QSOs, of which 2 in the SMC, were successfully matched. MACHO 061.08072.0358 was excluded because two VMC candidate sources are present, one at  $1.36''$  and one at  $1.49''$ . The mean distance of the VMC counterparts is  $0.86 \pm 0.29''$ .

With the exception of one QSO, as mentioned above, all known QSOs falling into VMC observed tiles were matched with the merged or un-merged catalogues. In the following analysis we consider only those found in the merged catalogue since the magnitudes of those in the un-merged catalogue may be influenced by the presence of bright neighbours.

#### 2.4. Summary of detected quasar sample

Table 2 lists the information about the 117 known quasars found in the merged VMC catalogue. The first column gives the QSOs name from the literature for which references are in column 2. Columns 3 and 4 list the J2000 coordinates of the VMC counterparts. The  $Y$ ,  $J$  and  $K_s$  magnitudes and 1 sigma uncertainties are listed in columns 5–10, where missing values are indicated with  $-99.999$ . Column 11 lists the VDFS source classification flag (1 for galaxies,  $-3$  for probable galaxies,  $-1$  for stars and  $-2$  for probable stars), column 12 the VMC tiles where QSOs were found and column 13 the photometric flag.

Of the 117 matched QSOs, 67 lie behind the LMC, 47 behind the SMC and 3 behind the Magellanic Bridge regions. The majority of the quasars are detected in all three wave bands,  $YJK_s$ , with 1 QSO present only in  $YJ$  data, 3 only in  $JK_s$  data and 2 only in  $K_s$  data. The VDFS pipeline classifies  $\sim 53\%$  of the matched QSOs as galaxies, among which two show clearly extended discs, and the other 47% as stars or probable stars.

For the 8 QSOs detected in the un-merged VMC catalogue, but blended with other sources which appear in the VMC merged catalogue, Table 3 lists the name, reference, wave bands and VMC tile in columns 1, 2, 3 and 4, respec-

**Table 3.** VMC blended quasars.

Name	Ref.	Filter	Tile
J004753.62-724350.6	7	$K_s$	SMC 4.3
J005444.70-724813.7	7	$K_s$	SMC 4.3
J005714.13-723342.8	7	$K_s$	SMC 5.4
MQS J051944.39-701957.3	8	$J, K_s$	LMC 5.5
MQS J052300.14-701831.7	8	$Y, K_s$	LMC 5.5
MQS J052431.88-702231.6	8	$K_s$	LMC 5.5
MQS J052908.79-702445.7	8	$J, K_s$	LMC 5.5
MQS J053304.31-714848.4	8	$K_s$	LMC 4.6

References as in table 2.

tively. These objects are listed for completeness but are not used in our analysis.

### 3. Results

#### 3.1. $YJK_s$ colour-colour diagram

##### 3.1.1. $YJK_s$ colour-colour diagram and known QSOs

Fig. 2 shows the distribution of the 117 known QSOs in the  $YJK_s$  colour-colour diagram superimposed to the distribution of sources detected in the LMC tile 8.8. This tile was chosen for comparison because it is located in the disc of the LMC but avoids the central region, where crowding influences the detection of sources rendering the sample with small photometric errors shallower than in the outer regions. In addition, the data for this tile are complete, i.e. all VMC epochs at each wave band have been obtained, reduced and included in the analysis. All 117 known QSOs are shown regardless of their quality flag and we have checked that the analysis of this paper does not change if only QSOs of photometric class A (Sect. 2) are used.

Most QSOs are located within the triangle limited by the following lines and the plotted region:

$$(J - K_s) = -1.25 \times (Y - J) + 1.05 \quad (1)$$

and

$$(J - K_s) = 2.05 \times (Y - J) - 0.15 \quad (2)$$

where the line

$$(J - K_s) = -1.25 \times (Y - J) + 1.90 \quad (3)$$

marks the division between star-like and galaxy-like QSOs. This line is parallel to the first line (Eq. 1) that defines a blue colour boundary beyond which no known QSOs are present. The other line (Eq. 2) runs parallel to the locus of stars and divides them from extra-galactic sources. The selection criteria that embrace the sample of known QSOs are not influenced by the choice of tile for the foreground sources which are only shown for the purpose of visualisation. Note that as well as the QSOs there are many other objects populating this region of the colour-colour space (on paper the eye may be drawn to not notice these well due to the denser grouping outside this area and the colours within it).

The highest concentrations of non-QSOs are attributed to main-sequence stars at the bluest colours and to giant stars of

**Table 2.** VMC quasar parameters.

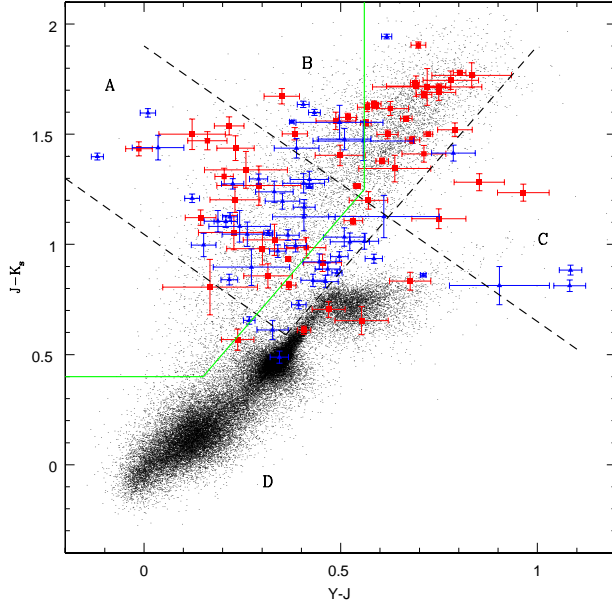
Name	Ref.	$\alpha$ (h : m : s)	$\delta$ (d : m : s)	$Y$ (mag)	$\sigma_Y$ (mag)	$J$ (mag)	$\sigma_J$ (mag)	$K_s$ (mag)	$\sigma_{K_s}$ (mag)	Class	Tile	Flag
OGLE 003850.79-731053.1	3	00:38:50.80	-73:10:53.4	16.562	0.006	16.142	0.006	14.878	0.006	-1	SMC 4.3	A
J003857.50-741000.7	10	00:38:57.53	-74:10:00.9	17.371	0.010	17.104	0.010	16.449	0.0123	-1	SMC 3.3	A
J003957.65-730603.6	7	00:39:57.64	-73:06:03.6	18.321	0.022	18.334	0.026	16.900	0.019	1	SMC 4.3	A
J004145.04-725435.9	7	00:41:45.04	-72:54:35.6	17.662	0.013	16.859	0.009	15.080	0.006	1	SMC 4.3	A
J004507.50-724121.8	7	00:45:07.55	-72:41:21.5	19.482	0.057	19.239	0.054	18.157	0.048	-2	SMC 4.3	A
J004520.77-730301.9	7	00:45:20.84	-73:03:01.6	-99.999	-99.999	19.968	0.100	18.709	0.074	1	SMC 4.3	A
J004522.89-724541.5	7	00:45:22.95	-72:45:41.4	19.934	0.085	19.767	0.085	18.961	0.093	1	SMC 4.3	A
J004551.62-725735.0	7	00:45:51.64	-72:57:35.0	19.169	0.044	18.781	0.037	17.345	0.025	-1	SMC 4.3	A
J004556.83-725636.5	7	00:45:56.80	-72:56:36.3	17.617	0.013	17.210	0.011	16.600	0.015	1	SMC 4.3	A
MACHO 208.15799.1085	2	00:47:15.92	-72:41:12.0	18.685	0.029	18.358	0.026	17.747	0.035	-1	SMC 4.3	A
J004736.12-724538.2	7	00:47:36.13	-72:45:38.1	18.864	0.034	18.514	0.030	16.842	0.019	1	SMC 4.3	A
J004818.76-732059.6	7	00:48:18.74	-73:21:40.1	19.419	0.053	18.910	0.041	17.432	0.027	-1	SMC 4.3	A
J004831.50-732339.9	7	00:48:31.50	-73:23:40.1	19.419	0.053	18.910	0.041	17.432	0.027	-1	SMC 4.3	A
J004944.41-725400.5	7	00:49:44.42	-72:54:00.3	-99.999	-99.999	-99.999	-99.999	17.201	0.023	-1	SMC 4.3	A
J004958.75-725952.2	7	00:49:58.86	-72:59:51.9	19.528	0.060	19.196	0.052	18.175	0.048	1	SMC 4.3	A
J005132.67-731411.6	7	00:51:32.66	-73:14:11.7	19.078	0.041	18.673	0.034	17.396	0.027	-1	SMC 4.3	A
J005203.27-723830.6	7	00:52:03.30	-72:38:30.6	19.948	0.088	19.451	0.066	17.898	0.039	-1	SMC 4.3	A
J005235.03-732940.6	7	00:52:34.94	-73:29:40.9	20.235	0.112	19.331	0.059	18.518	0.064	-1	SMC 4.3	B
J005254.15-725628.1	7	00:52:54.23	-72:56:28.1	19.257	0.047	18.546	0.031	17.135	0.022	1	SMC 4.3	A
J005259.10-724510.9	7	00:52:59.08	-72:45:10.8	19.812	0.080	19.520	0.071	18.253	0.053	1	SMC 4.3	A
J005402.17-742733.3	10	00:54:02.24	-74:27:33.4	18.243	0.017	17.726	0.0148	16.149	0.011	1	SMC 3.3	B
J005433.79-730924.0	7	00:54:33.82	-73:09:24.1	20.171	0.104	19.614	0.075	18.144	0.048	-1	SMC 4.3	A
J005454.05-723726.2	7	00:54:53.97	-72:37:26.5	19.402	0.054	18.849	0.040	18.195	0.050	1	SMC 4.3	A
J005511.81-723728.3	7	00:55:11.78	-72:37:28.4	19.241	0.047	18.454	0.029	17.040	0.021	-1	SMC 4.3	A
J005517.63-712655.1	10	00:55:17.72	-71:26:55.2	18.325	0.017	17.741	0.014	16.805	0.015	-1	SMC 5.4	B
MACHO 207.16316.446	2	00:55:34.67	-72:28:34.3	17.335	0.009	17.454	0.012	16.055	0.010	-1	SMC 5.4	A
J005708.12-722257.8	7	00:57:08.13	-72:22:57.8	19.398	0.036	18.608	0.025	17.088	0.018	1	SMC 5.4	A
OGLE 005719.84-722533.5	4	00:57:19.82	-72:25:34.0	17.151	0.008	16.463	0.007	14.728	0.006	1	SMC 5.4	A
J005754.26-715630.7	10	00:57:54.33	-71:56:30.8	18.133	0.015	17.435	0.011	15.531	0.008	1	SMC 5.4	A
J005901.04-721330.0	7	00:59:00.94	-72:13:30.0	19.486	0.039	18.915	0.030	17.715	0.026	1	SMC 5.4	A
J010005.10-715921.7	7	01:00:05.13	-71:59:21.5	19.108	0.029	18.870	0.030	18.302	0.038	1	SMC 5.4	A
J010005.70-715723.5	7	01:00:05.70	-71:57:23.4	18.900	0.024	17.816	0.015	16.933	0.016	-1	SMC 5.4	A
J010031.06-722444.1	7	01:00:31.05	-72:24:44.4	-99.999	-99.999	17.890	0.015	17.066	0.018	-2	SMC 5.4	A
J010046.02-722131.4	7	01:00:46.02	-72:21:31.2	-99.999	-99.999	18.600	0.024	17.134	0.018	1	SMC 5.4	A
J010057.77-722230.8	7	01:00:57.77	-72:22:31.0	19.492	0.039	19.005	0.033	17.445	0.022	1	SMC 5.4	A
J010127.75-721306.2	7	01:01:27.81	-72:13:06.4	19.437	0.037	19.025	0.033	18.040	0.032	1	SMC 5.4	A
OGLE 010131.45-720702.6	4	01:01:31.45	-72:07:03.1	18.308	0.017	17.964	0.016	17.476	0.022	-1	SMC 5.4	A
J010137.52-720418.9	7	01:01:37.50	-72:04:19.1	18.175	0.015	17.463	0.012	15.783	0.009	1	SMC 5.4	A
J010241.90-723238.7	7	01:02:41.90	-72:32:38.8	17.885	0.013	17.875	0.015	16.278	0.012	-1	SMC 5.4	B
OGLE 010244.89-721521.7	3	01:02:44.90	-72:15:22.0	17.925	0.013	17.707	0.013	16.582	0.014	-1	SMC 5.4	A
J010507.66-712448.4	10	01:05:07.68	-71:24:48.4	17.933	0.013	17.347	0.011	15.710	0.009	1	SMC 5.4	B
OGLE 010522.51-715649.7	4	01:05:22.54	-71:56:49.9	18.334	0.017	17.838	0.015	16.893	0.016	-1	SMC 5.4	A
J010650.81-713253.0	10	01:06:50.90	-71:32:53.0	17.871	0.013	17.749	0.014	16.540	0.013	-1	SMC 5.4	A
OGLE 010656.98-722448.1	4	01:06:56.99	-72:24:48.4	18.489	0.019	17.922	0.016	16.299	0.012	1	SMC 5.4	A
OGLE 010717.66-722418.3	4	01:07:17.73	-72:24:18.3	19.674	0.045	19.443	0.045	18.240	0.037	1	SMC 5.4	A
QJ0116-7259	9	01:16:33.51	-72:59:49.7	17.719	0.010	17.155	0.009	15.603	0.011	1	SMC 4.5	A
J011652.81-740050.8	10	01:16:52.85	-74:00:50.8	17.455	0.010	16.964	0.008	16.093	0.111	-1	SMC 3.5	A
1WGA J0216.6-7331	6	02:16:44.57	-73:31:40.5	18.212	0.015	17.995	0.015	17.155	0.019	-1	BRI 2.3	A
1WGA J0217.7-7347	6	02:17:45.11	-73:47:23.3	19.038	0.024	18.655	0.021	17.153	0.019	1	BRI 2.3	A
PKS0333-729	6	03:32:42.95	-72:49:04.4	18.648	0.020	18.496	0.024	17.499	0.048	-1	BRI 3.7	A
MACHO 42.00860.123	2	04:46:10.96	-72:05:10.0	16.522	0.005	15.812	0.005	14.952	0.006	-1	LMC 4.2	A
MACHO 53.03360.344	2	05:00:53.98	-66:44:00.0	18.563	0.018	18.178	0.021	17.184	0.019	-1	LMC 8.3	B
MACHO 25.03469.117	2	05:01:46.72	-67:32:40.1	17.122	0.009	16.505	0.009	14.561	0.005	-1	LMC 7.3	A
MACHO 25.3712.72	2	05:02:53.73	-67:25:45.3	17.332	0.010	16.899	0.011	15.300	0.008	-1	LMC 7.3	A
J050303.97-663345.9	10	05:03:04.0	-66:33:46.0	15.395	0.003	14.806	0.003	13.173	0.003	1	LMC 8.3	A
MACHO 53.3970.140	2	05:04:35.99	-66:24:15.9	17.065	0.007	16.749	0.009	15.696	0.009	-1	LMC 8.3	A
J050550.35-675017.5	5	05:05:50.40	-67:50:18.0	16.995	0.008	16.272	0.008	14.772	0.006	1	LMC 7.3	A
OGLE 050736.52-684751.7	1	05:07:36.44	-68:47:51.6	18.204	0.040	18.168	0.052	16.729	0.023	-1	LMC 6.4	B
MACHO 52.4565.0356	2	05:08:30.62	-67:02:28.9	17.856	0.014	17.564	0.018	16.268	0.015	-1	LMC 7.3	A
OGLE 050833.29-685427.5	1	05:08:33.21	-68:54:27.3	17.977	0.033	17.816	0.038	16.345	0.017	1	LMC 6.4	A

Table 2. continued.

Name	Ref.	$\alpha$ (h : m : s)	$\delta$ (d : m : s)	$Y$ (mag)	$\sigma_Y$ (mag)	$J$ (mag)	$\sigma_J$ (mag)	$K_s$ (mag)	$\sigma_{K_s}$ (mag)	Class	Tile	Flag
MQS J050842.68-690959.4	8	05:08:42.67	-69:09:59.5	18.723	0.064	18.423	0.064	17.441	0.039	1	LMC 6_4	A
MACHO 20.4678.600	2	05:08:54.13	-67:37:34.2	18.974	0.032	18.642	0.035	17.403	0.033	-1	LMC 7_3	B
J050900.76-672114.1	5	05:09:00.67	-67:21:14.1	18.704	0.027	18.144	0.025	17.130	0.027	-1	LMC 7_3	B
J050915.35-695417.3	10	05:09:15.37	-69:54:17.3	16.721	0.012	16.054	0.009	4.482	0.005	1	LMC 6_4	B
OGLE 050924.05-672124.1	1	05:09:23.77	-67:21:24.5	17.793	0.014	17.110	0.013	15.636	0.010	1	LMC 7_3	B
J050940.60-685320.6	5	05:09:40.53	-68:53:20.3	17.934	0.032	17.465	0.027	16.760	0.023	1	LMC 6_4	A
MACHO 5.4892.1971	2	05:10:32.39	-69:27:15.7	18.106	0.036	17.652	0.032	16.736	0.022	1	LMC 6_4	A
MQS J051045.85-694126.5	8	05:10:45.84	-69:41:26.4	18.097	0.036	17.676	0.033	16.381	0.017	-1	LMC 6_4	A
MQS J051049.16-692851.9	8	05:10:49.15	-69:28:51.8	19.397	0.114	18.677	0.079	16.962	0.026	1	LMC 6_4	A
MQS J051159.38-694726.1	8	05:11:59.33	-69:47:25.8	18.894	0.074	18.257	0.054	16.912	0.026	1	LMC 6_4	A
J051244.64-693857.2	5	05:12:44.54	-69:38:57.1	17.605	0.024	16.855	0.016	15.143	0.008	1	LMC 6_4	A
MQS J051345.50-690636.9	8	05:13:45.45	-69:06:37.1	18.615	0.057	17.866	0.039	16.750	0.023	1	LMC 6_4	A
MQS J051404.81-694446.6	8	05:14:04.80	-69:44:46.5	18.690	0.061	17.998	0.043	16.280	0.016	1	LMC 6_4	A
J051433.58-693245.7	5	05:14:33.45	-69:32:45.6	17.466	0.021	17.100	0.020	16.058	0.013	-1	LMC 6_4	A
MQS J051534.35-685422.2	8	05:15:34.35	-68:54:22.1	19.054	0.086	18.221	0.053	16.454	0.018	1	LMC 6_4	A
MQS J051547.78-700002.3	8	05:15:47.77	-70:00:02.2	18.798	0.068	18.525	0.069	17.628	0.046	-1	LMC 6_4	A
MACHO 78.5855.788	2	05:16:26.31	-69:48:19.2	17.360	0.019	17.135	0.021	15.860	0.012	-1	LMC 6_4	A
MACHO 2.5873.82	2	05:16:28.84	-68:37:02.3	16.052	0.007	15.511	0.006	14.247	0.005	1	LMC 6_4	A
MQS J051716.95-704402.0	8	05:17:16.93	-70:44:02.2	17.332	0.013	16.727	0.010	15.348	0.008	1	LMC 5_5	B
MQS J051739.83-695705.3	8	05:17:39.80	-69:57:05.2	18.883	0.073	18.623	0.076	17.285	0.035	1	LMC 6_4	A
MQS J051746.88-685458.1	8	05:17:46.88	-68:54:58.0	18.543	0.055	18.420	0.065	16.921	0.026	1	LMC 6_4	A
MQS J051834.75-703751.3	8	05:18:34.74	-70:37:51.2	19.152	0.055	18.300	0.033	17.018	0.021	1	LMC 5_5	A
OGLE 051853.19-690217.7	1	05:18:53.08	-69:02:17.5	19.367	0.113	18.757	0.085	17.631	0.046	-1	LMC 6_4	B
MQS J051856.04-701743.6	8	05:18:56.05	-70:17:43.7	18.670	0.036	17.588	0.019	16.775	0.018	-1	LMC 5_5	A
MQS J051912.33-710914.6	8	05:19:12.29	-71:09:14.6	18.850	0.042	18.185	0.030	-99.999	-99.999	1	LMC 5_5	B
MQS J051916.98-704458.8	8	05:19:16.96	-70:44:58.8	18.187	0.024	17.726	0.021	16.894	0.019	-1	LMC 5_5	A
MQS J051953.65-704622.7	8	05:19:53.63	-70:46:22.6	19.323	0.063	19.095	0.064	18.041	0.043	1	LMC 5_5	A
MQS J052037.03-705100.1	8	05:20:37.01	-70:51:00.1	18.737	0.037	18.111	0.028	16.494	0.015	1	LMC 5_5	A
MACHO 6.6572.268	2	05:20:56.97	-70:24:52.7	17.425	0.013	17.031	0.013	16.305	0.013	-1	LMC 5_5	A
J052141.75-703029.2	5	05:21:41.61	-70:30:28.8	18.281	0.026	18.137	0.029	17.015	0.021	1	LMC 5_5	A
MACHO 13.6805.324	2	05:22:47.18	-71:01:30.7	18.160	0.023	17.731	0.020	16.894	0.019	-1	LMC 5_5	A
MACHO 13.6808.521	2	05:22:47.68	-70:47:34.8	18.175	0.024	17.708	0.021	16.819	0.018	-1	LMC 5_5	A
MQS J052312.95-701529.8	8	05:23:12.94	-70:15:29.7	18.037	0.021	17.418	0.017	15.919	0.010	1	LMC 5_5	A
MQS J052335.33-710758.1	8	05:23:35.33	-71:07:58.1	19.257	0.057	18.293	0.032	17.059	0.021	1	LMC 5_5	A
MQS J052336.58-710033.9	8	05:23:36.58	-71:00:33.9	18.910	0.043	18.234	0.031	17.401	0.027	1	LMC 5_5	A
MQS J052354.44-704821.9	8	05:23:54.42	-70:48:21.9	-99.999	-99.999	-99.999	-99.999	17.497	0.029	1	LMC 5_5	A
MQS J052408.88-704812.8	8	05:24:08.87	-70:48:12.8	18.834	0.041	18.325	0.034	17.291	0.025	-1	LMC 5_5	A
MQS J052444.07-702601.9	8	05:24:44.07	-70:26:01.9	18.757	0.039	18.234	0.031	17.222	0.024	-1	LMC 5_5	A
MQS J052502.45-705023.0	8	05:25:02.47	-70:50:23.1	18.967	0.045	18.705	0.045	17.658	0.032	-1	LMC 5_5	A
MQS J052521.42-710932.2	8	05:25:21.42	-71:09:32.2	19.292	0.060	18.885	0.053	17.761	0.035	-1	LMC 5_5	A
MQS J052528.91-700448.6	8	05:25:28.82	-70:04:48.3	17.434	0.014	17.067	0.013	16.252	0.013	1	LMC 5_5	A
MQS J052529.65-701018.9	8	05:25:29.65	-70:10:18.9	18.918	0.044	18.602	0.043	17.746	0.035	1	LMC 5_5	A
MQS J052705.98-702610.7	8	05:27:05.89	-70:26:11.2	18.522	0.032	18.076	0.028	17.155	0.023	-1	LMC 5_5	A
MQS J052745.26-700533.9	8	05:27:45.26	-70:05:33.9	17.973	0.020	17.765	0.022	16.662	0.017	-1	LMC 5_5	A
MQS J052747.29-711058.9	8	05:27:47.29	-71:10:59.0	19.267	0.059	18.487	0.038	16.742	0.017	1	LMC 5_5	A
MQS J052749.08-703641.7	8	05:27:49.09	-70:36:42.1	17.843	0.018	17.311	0.015	16.202	0.012	1	LMC 5_5	A
MQS J052931.17-702958.7	8	05:29:31.19	-70:29:58.7	19.048	0.049	18.549	0.041	17.145	0.023	1	LMC 5_5	A
MQS J053044.94-712358.5	8	05:30:44.92	-71:23:58.5	18.527	0.032	18.175	0.030	16.978	0.021	-1	LMC 5_5	B
MQS J053120.33-715326.0	8	05:31:20.33	-71:53:26.0	18.054	0.015	17.714	0.014	16.744	0.025	-1	LMC 4_6	B
MQS J053225.83-713328.6	8	05:32:25.74	-71:33:28.5	19.153	0.032	18.921	0.035	17.483	0.044	1	LMC 4_6	B
MQS J053708.16-721747.5	8	05:37:08.15	-72:17:47.5	17.542	0.011	17.138	0.010	15.502	0.010	-1	LMC 4_6	A
MQS J053741.18-715945.8	8	05:37:41.18	-71:59:45.7	18.546	0.021	18.139	0.019	16.969	0.029	-1	LMC 4_6	A
MQS J054200.63-714011.4	8	05:42:00.63	-71:40:11.4	18.741	0.024	18.554	0.025	17.448	0.041	-1	LMC 4_6	A
MQS J054227.27-720454.7	8	05:42:27.33	-72:04:54.4	19.319	0.036	18.570	0.025	16.880	0.026	1	LMC 4_6	A
MQS J054319.60-715151.8	8	05:43:19.59	-71:51:51.8	18.874	0.026	18.658	0.027	17.120	0.031	1	LMC 4_6	A
RXS J05466-6415	6	05:46:41.84	-64:15:22.0	15.522	0.004	15.147	0.004	13.590	0.004	-1	LMC 9_7	A
MACHO 75.13376.66	2	06:02:34.32	-68:30:41.5	18.127	0.016	17.924	0.017	16.615	0.034	1	LMC 6_8	A

References. (1) Dobrzycki et al. (2002); (2) Geha et al. (2003); (3) Dobrzycki et al. (2003a); (4) Dobrzycki et al. (2003b); (5) Dobrzycki et al. (2005); (6) Véron-Cetty & Véron (2010); (7) Kozłowski et al. (2011); (8) Kozłowski et al. (2012); (9) Tinney et al. (1997); (10) Kamath et al. (in prep.).





**Fig. 2.** Colour-colour diagram showing the known QSOs where in red (filled squares) are those classified as galaxy-like and in blue (filled triangles) those classified as star-like by the VDFS pipeline. All sources from the LMC tile 8\_8 with photometric errors  $< 0.1$  mag and quality flags = 0 in each wave band are shown with black dots. Dashed black lines identify the regions where known QSOs are found. In particular, region A is dominated by QSOs with a stellar morphology and region B by QSOs with a detectable host galaxy, i.e. galaxy morphology. The LMC and MW stellar populations dominate region D. The green continuous line encloses the region identified in Paper II to contain PNe.

the LMC. The plume of sources with  $(Y - J) > 0.5$  mag belongs to the MW foreground. Source at  $(Y - J) \sim 0.6$  mag and  $(J - K_s) \sim 1.5$  mag are mostly background galaxies. It is interesting to note that QSOs morphologically classified as galaxy-like from VMC data dominate region B while those classified as star-like are mostly located in region A blueward from it. In addition, many star-like QSOs are redder than the green sloped line delimiting the region where most planetary nebulae (PNe) are found (Miszalski et al, 2011a, hereafter Paper II). Only a handful of QSOs occupy region C. The number of sources in this region does increase in the presence of interstellar reddening like in the case of tile LMC 6\_6 (Table 4). QSOs located outside regions ABC, i.e. in region D, cannot be distinguished from LMC and MW stars by their  $YJK_s$  colours. Their number is, however, small. It would be worthwhile to explore the presence of QSOs in the region resulting from the intersection of region D and that defined by PNe.

Based on the number of known QSOs distributed in regions A&B (Fig. 2), 65% and 21% of objects classified as star-like occupy these regions respectively, whilst the relative percentages of galaxy-like QSOs are 35% and 79%. Outside regions A&B lie  $\sim 16\%$  of the QSOs, with half classified as star-like and half as galaxy-like.

The  $YJK_s$  colour-colour diagram (Fig. 2) represents the best VMC diagram to distinguish the bulk of back-

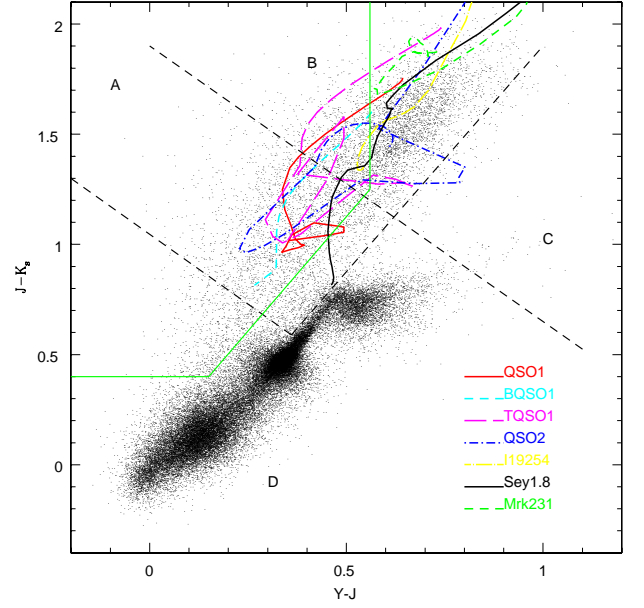


**Fig. 3.** Colour-colour diagram showing the distribution of sources in tile LMC 8\_8 with photometric errors  $< 0.1$  mag and quality flags = 0 in each wave band (black dots). Superimposed are models from the SWIRE template library (Polletta et al. 2007). The green and dashed black lines are as in Fig. 2. Most QSOs lie in regions A and B.

ground QSOs from the foreground stellar population of the Magellanic Clouds and the MW. It also provides a clear indication of the location of normal galaxies that contaminate the QSO sample. We note that the first part of the KX method to select QSOs (Maddox et al. 2012) instead involves  $gJK$ , and in a sense our step is similar except using  $Y$  instead of  $g$ , not least because we have  $Y$ , but not  $g$ , data of appropriate depth. For a similar distribution in the  $VJK$  colour-colour diagram see Warren, Hewett & Foltz (2000).

### 3.1.2. $YJK_s$ colour-colour diagram and QSO model templates

QSO templates obtained from Spitzer-space-telescope Wide-field InfraRed Extragalactic (SWIRE) project template library by Polletta et al. (2007) have been convolved with the VISTA spectral response over each of the  $YJK_s$  filters and the location of these QSOs is shown in Fig. 3, superimposed on the distribution of sources in tile LMC 8.8 as in Fig. 2. The average redshift from the QSO models (excluding I19254 and Sey 1.8) is  $1.22 \pm 0.25$  in region A and  $0.44 \pm 0.25$  in region B. This is consistent with the trends presented in Sect. 3.3.

The template models are semi-empirical, i.e. they have been constructed combining observational data for similar objects. Those shown in Fig. 3 refer to three type 1 QSOs, one type 2 QSO and two obscured QSOs as well as a moderately luminous AGN. The QSO1 templates were derived from the combination of SDSS spectra and rest-frame IR data where QSO1, TQSO1 and BQSO1 refer to the average flux of all, the highest 25% and the lowest 25% of the measurements, respectively. The QSO2 template was obtained by combining



a optical/near-IR spectrum with the rest-frame IR data. The AGN template, Seyfert 1.8, is the result of broad-band photometric data and spectra from the Infrared Space Observatory while the templates Mrk 231 and IRAS 19254-7245 South (I19254) are fits to their composite, AGN plus starburst, spectral energy distributions.

Regions A+B where most known QSOs are found (Fig. 2) are well matched by the models and a few QSOs may be found also in region C.

### 3.1.3. Correction for reddening

The QSOs and stars in the Magellanic Clouds as well as stars in the MW are reddened by interstellar dust present along the line of sight and the effect of reddening has been checked as follows. Reddening values in terms of  $E(V - I)$  were extracted from the extinction map from Haschke et al. (2011) for all but 10 (located outside the map) of the 117 QSOs. Using the Cardelli, Clayton and Mathis (1989) extinction law, the average QSO extinction is  $A(Y) = 0.045$  mag,  $A(J) = 0.032$  and  $A(K_s) = 0.013$  mag. The estimated reddening, while accounting for the MW and LMC components, does not account for the intergalactic dust that lies between the LMC and the QSOs and for dust in the torus surrounding the AGN.

The stellar population shown in Fig. 2 corresponds to the LMC and MW stars located in tile LMC 8.8. This tile is outside the region studied by Haschke et al. (2011). Therefore, reddening values were extracted from the Zaritsky et al. (2004) extinction map. Here, instead of de-reddening each individual star, an average value referring to cool stars only,  $A(V) = 0.35$  mag, was obtained in a region centred on the tile and with a radius of  $12'$ . Cool stars were chosen because they have similar characteristics to red clump giant and RR Lyrae stars used by Haschke et al. (2011). The size of the region, whilst being smaller than the extent of a tile, is representative of the average extinction since this tile is located in the outer disc of the LMC where the reddening is uniform. By applying the extinction law from Cardelli et al. (1989) extinction values of  $A(Y) = 0.14$  mag,  $A(J) = 0.10$  mag and  $A(K_s) = 0.04$  mag were derived. These values may be too high since Haschke et al. (2011) found that in the less populated regions of the LMC differences in  $E(V - I)$  between their extinction map and that of Zaritsky et al. (2004) amount to  $0.07 - 0.10$  mag on average. In addition, while these values are applicable to LMC stars they are certainly too high towards foreground MW stars and too low towards extra-galactic sources.

In view of the uncertainty in the extinction of LMC tile 8.8 outlined in the previous paragraph, the Schlegel, Finkbeiner & Davis (1998) extinction map based on DIRBE/IRAS mid-IR observations was used to find average reddening and extinction,  $E(B - V) = 0.067$  and  $A(V) = 0.207$  mag, in a region of  $2 \text{ deg}^2$  in size centred on tile LMC 8.8. The extinction value is consistent with the mean value,  $A(V) = 0.187 \pm 0.040$  mag, derived in Paper IV from the recovering of the star formation history.  $A(Y) = 0.083$  mag,  $A(J) = 0.058$  mag and  $A(K_s) = 0.024$  mag are then obtained. These values are  $0.02 - 0.06$  mag smaller than those derived from the Zaritsky et al. (2004) extinction map. Using the TRILEGAL code (Girardi et al. 2005) to simulate the MW population we obtain that it accounts for  $A(V) = 0.05$  of absorption implying that most of the reddening towards the LMC is due to the galaxy itself.

The un-reddened colours of QSOs and stars show that the boundaries are not significantly affected and the standard deviation of the reddening values was about as high as the values themselves, so we do not apply any reddening correction in our analysis.

### 3.2. Colour-magnitude diagrams

The distribution of known QSOs in the VMC colour-magnitude diagrams (CMDs) is shown in Fig. 4 superimposed on the distribution of LMC and MW sources present in tile LMC 8.8.

The  $(Y - J)$  vs.  $Y$  or  $J$  CMDs show that QSOs overlap with the stellar populations of the LMC and of the MW that is also not distinguishable from LMC stars. The  $(Y - K_s)$  vs.  $Y$  or  $K_s$  CMDs provide the best separation between the LMC and MW stellar population as well as background galaxies. QSOs, however, especially those with a stellar morphology, do overlap with MW stars. The  $(J - K_s)$  vs.  $J$  or  $K_s$  CMDs offer instead the best separation between QSOs and stars of the MW or LMC. In the  $(J - K_s)$  vs.  $K_s$  CMD, galaxy-like QSOs do overlap with the cone of galaxies (with base  $1 < (J - K_s) < 2$  mag and vertex at  $(J - K_s) \sim 1.5$  mag); see Kerber et al. (2009), while star-like QSOs seem well separated from it.

The distribution of known QSOs in the CMDs unsurprisingly indicates that the present sample is magnitude limited and that the VMC data potentially improves the magnitude limit for finding candidates fainter than the present known sample QSOs by  $> 1$  mag.

### 3.3. Trends with redshift

Figure 5 shows the distribution of redshifts with respect to VMC magnitudes and colours. There appears to be no trend as a function of magnitude nor of  $(Y - J)$  colour. The QSOs occupy the whole of the parameter space delimited on one side by the bright limit of the survey and on the other by the faint limit of the present sample. The faint limit is also influenced by the incomplete observations of  $K_s$  epochs.

The plots of redshift as a function of  $(J - K_s)$  and  $(Y - K_s)$  colours suggest a trend of larger redshifts at smaller colours. This indicates that QSOs at small redshifts are redder than QSOs at larger redshifts as predicted by Maddox & Hewett (2006). These authors simulated the evolution of quasars in the near-IR and found them getting bluer as redshift goes from 0 to 3. Figure 5 also shows a dichotomy between star-like and galaxy-like QSOs where the latter are concentrated at small redshifts as in Maddox et al. (2008).

### 3.4. Variability from $K_s$ photometry

The VMC survey provides at least 12 epochs in  $K_s$  observed under similar observing conditions (Paper I). Additional epochs may, however, be obtained in worse conditions. The number of epochs currently available (Table 1) is not sufficient to sample in detail a QSO light-curve but the accuracy of the photometry is enough to detect significant variability.

The light-curves for each known QSO from the presently available VMC data are shown in the Appendix. Measurements obtained during the same night, excluding those that do not meet the observing constraints have been av-

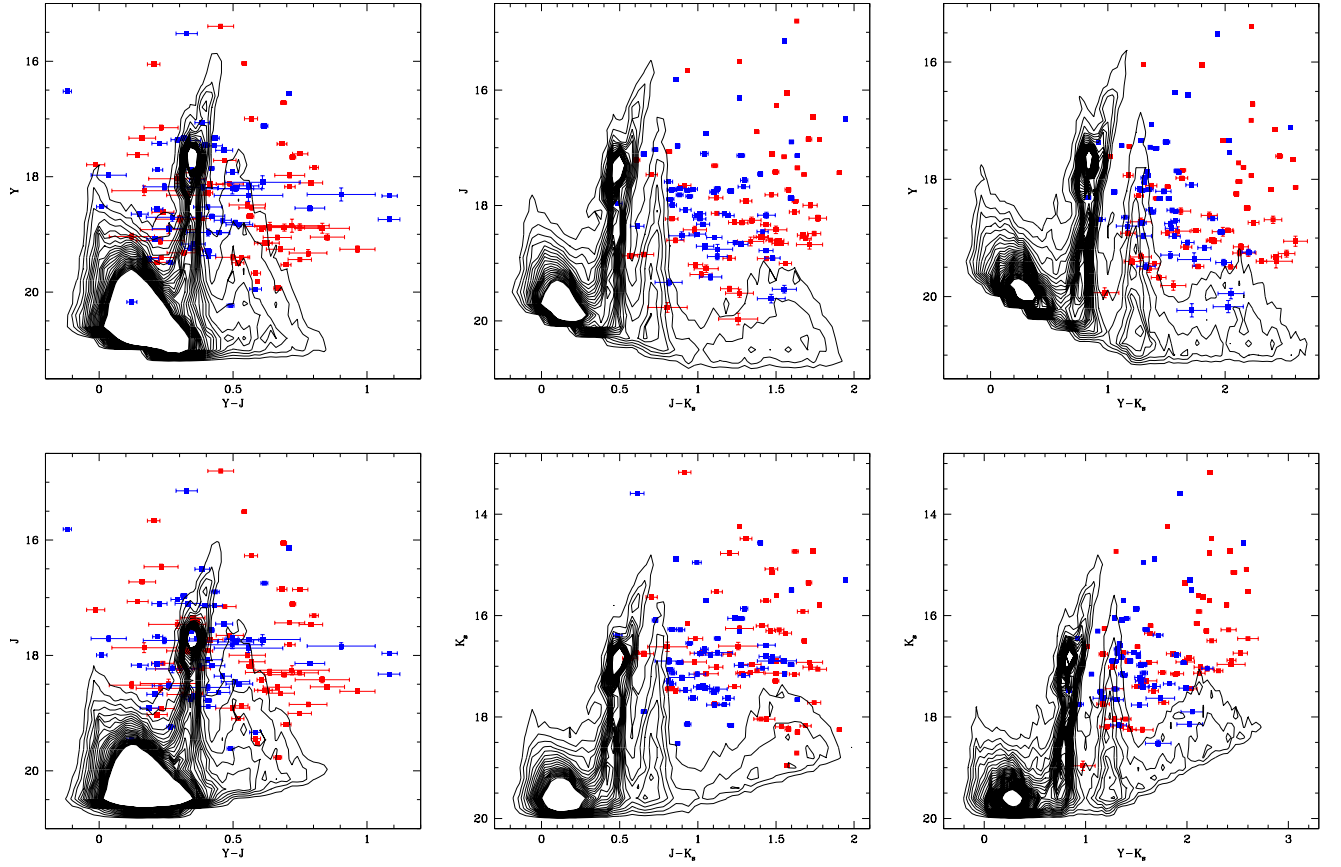


**Fig. 4.** Hess diagrams of sources in tile LMC 8.8 with photometric errors  $< 0.1$  mag and quality flags = 0, in each pair of two wave bands, shown as contour plots. The known QSOs behind the Magellanic system are displayed as squares. QSOs are colour coded as in Fig. 2.

eraged and the error bar corresponds to the standard deviation of the mean. We refer to the  $\sim 39\%$  /  $\sim 27\%$  /  $\sim 33\%$  of the known QSO light-curves sampled over 300 – 600/40 – 80/shorter days as the long/mid/short-range samples. The current short sample includes some single epoch observations. The acquisition of  $K_s$  band epochs for most VMC tiles is still on-going (Table 1).

An example of QSO  $K_s$  light-curve is shown in Fig. 6. The shapes of the light-curves are in general irregular without any clear periodicity. There is often a changing brightness as a function of time both in the long- and mid-range samples. Peaks superimposed on this trend are in some cases significant with respect to the error bars. On average there are broad (up to 100 days wide) and narrow (20 – 40 days wide) peaks. Curves of the mid-range sample appear noisier but this is largely an effect of the more frequent sampling compared to the long-range sample. Long-range curves do show a similar behaviour in the time range where more data points are available.

To quantify the variation the slope in the  $K_s$  band has been derived for each known QSO and the number distribution of the slope values is shown in Fig. 7. There is a narrow peak due to sources with Slope  $\sim 0$  mag/day while most of the sample has  $1 < \text{Slope} < 3.5 \times 10^{-4}$  mag/day. Only with a larger sample of QSOs we will be able to establish if the latter is consistent with a decreasing gaussian function or represents a bump in the distribution. The remaining QSOs define a constant tail out

to Slope  $\sim 10^{-3}$  mag/day. In summary  $\sim 75\%$  of the presently known QSOs have Slope  $> 10^{-4}$  mag/day. In the next section we will explore the potential of using  $K_s$  variability, along with the colour regions given above, as a discriminant for candidate QSOs.

### 3.5. Selection of candidate QSOs

#### 3.5.1. Expected number of QSOs

In a given  $1.5 \text{ deg}^2$  VMC tile we expect 17 QSOs with  $i < 19$  mag (Schneider et al. 2010). The approximate  $i$  band magnitude corresponding to a given  $K_s$  band magnitude has been calculated assuming that the  $\sim 2.5$  mag difference between the tip of the red giant branch (TRGB) at  $K_s$  and at  $I$  is applicable to other sources and that there is not a major difference between the  $i$  and  $I$  filters. The TRGB in the LMC occurs at  $K_s = 12$  mag and at  $I = 14.54$  mag (Cioni et al. 2000). The VMC survey, however, can probe fainter magnitudes (see Fig. 4) and the number of QSO candidates is therefore larger.

Tile LMC 5.5 is entirely within the area where the known QSO sample is complete to  $I < 19.2$  mag (Kozłowski et al. 2012) and in this tile the faintest known QSO (MQS J051953.65 – 704622.7) has VMC magnitudes  $Y = 19.32$ ,  $J = 19.09$ ,  $K_s = 18.04$  mag. The numbers of known QSOs in regions A, B and C of tile LMC 5.5 are listed in Table 4

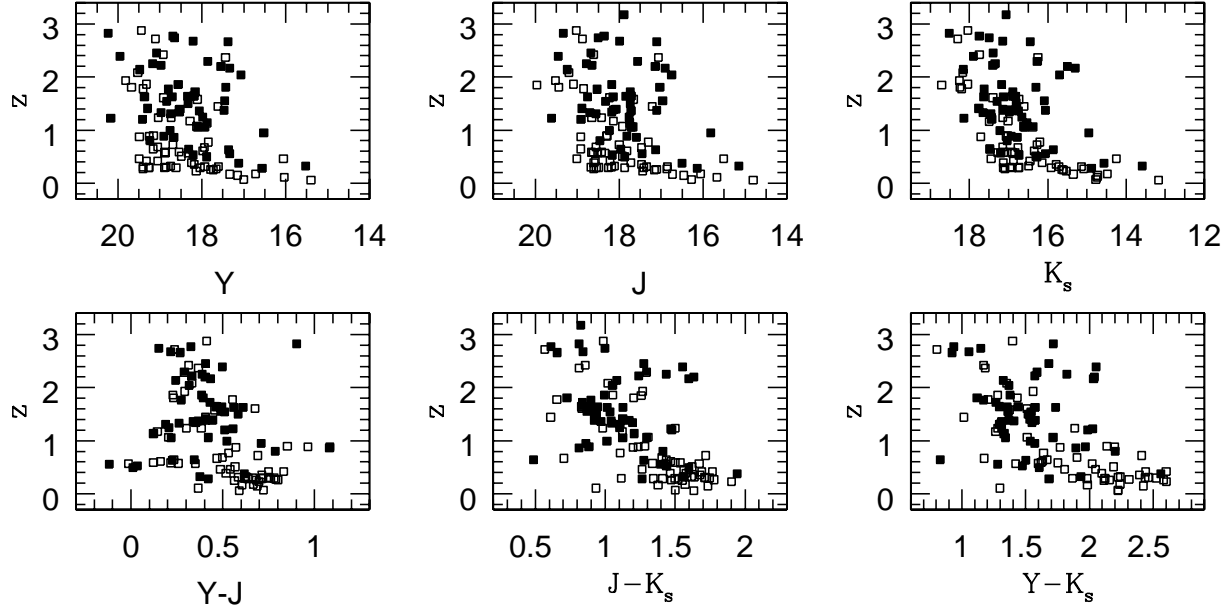


**Fig. 5.** Distribution of redshift versus magnitudes (top line) and colours (bottom line) for known QSOs behind the Magellanic system. Filled symbols indicate sources classified as star-like by the VDFS pipeline and empty symbols those classified as galaxies. Note the possible trend of redshift as a function of  $(J - K_s)$  and  $(Y - K_s)$  colours, and the concentration of galaxy type objects with small redshift at red colours.

along with related information for the two other completed tiles 6\_6 and 8\_8, together with the number of objects brighter than these limits in each tile and with photometric errors  $< 0.1$  mag and quality flags = 0 in each wave band. Even with the small number statistics it is clear that galaxy-like QSOs dominate region B and star-like QSOs dominate region A in these three tiles.

By taking the ratio of all sources lying in colour selected regions A & B (Fig. 2) found down to the same magnitude as the faintest and with the same photometric and quality flags to the number of known QSOs, it appears that  $\sim 6\%$  of all sources in tile LMC 5\_5 are known QSOs. Those in region C, may be influenced by reddened LMC sources and so their percentage should be considered as an upper limit. Using this information it is possible to extrapolate the number of QSOs VMC may expect to find in the other tiles.

Using Table 4, we now analyse the other two LMC tiles for which VMC observations are completed. Tile LMC 6\_6 includes the 30 Doradus regions where the reddening is the highest within the LMC implying the presence of many reddened LMC sources in region C. Tile LMC 6\_6 contains more sources than tile LMC 8\_8, on average, because of it is nearer to the centre of the galaxy, but the difficulty in detecting them clearly results in larger photometric errors and quality flags. This explains the inferior number of sources selected to have photometric errors  $< 0.1$  mag and quality flags = 0 in each wave band. Taking all objects in colour regions A & B and assuming the same percentage of known QSOs, as derived from tile LMC 5\_5, we find the number of QSOs VMC might expect to detect is 13 in tile LMC 6\_6 and 30 in tile LMC 8\_8.

**Table 4.** VMC quasar candidates.

Sources	Tile	Region A <sup>a</sup> gal. + star	Region B <sup>a</sup> gal. + star	Region C <sup>a</sup> gal. + star
No. QSOs	LMC 5_5	4 + 8	5 + 0	2 + 1
Mag. Lim.	LMC 5_5	137 + 29	140 + 3	14 + 21
QSOs %	LMC 5_5	2.9 + 27.6	3.6 + 0	14.3 + 4.8
Mag. Lim.	LMC 6_6	86 + 28	97 + 7	152 <sup>b</sup> + 845 <sup>b</sup>
Exp. No. QSOs	LMC 6_6	2 + 8	3 + 0	22 <sup>b</sup> + 40 <sup>b</sup>
Var. QSO cand.	LMC 6_6	15	11	49 <sup>b</sup>
Mag. Lim.	LMC 8_8	129 + 55	317 + 1	3 + 12
Exp. No. QSOs	LMC 8_8	4 + 15	11 + 0	0 + 1
Var. QSO cand.	LMC 8_8	14	7	1

<sup>a</sup> Regions ABC are those in Fig. 2.

<sup>b</sup> Includes reddened LMC stars.

<sup>c</sup> Mag. Lim. corresponds to the No. objects with  $Y < 19.32$  mag,  $J < 19.09$  mag and  $K_s < 18.04$  mag, photometric errors  $< 0.1$  mag and quality flags = 0 in each wave band.

### 3.5.2. Candidate QSOs from $YJK_s$ colour-colour diagram and $K_s$ variability

We showed above that most known QSOs lie in regions A+B of the  $YJK_s$  colour-colour diagram. However, the many other objects in the same region of colour space at first sight implies that spectroscopic follow up of the sample will produce only  $\sim 6\%$  which are actually QSOs, but we can also use the known  $K_s$  variability over timescales of 40 – 600 days for 75% of the

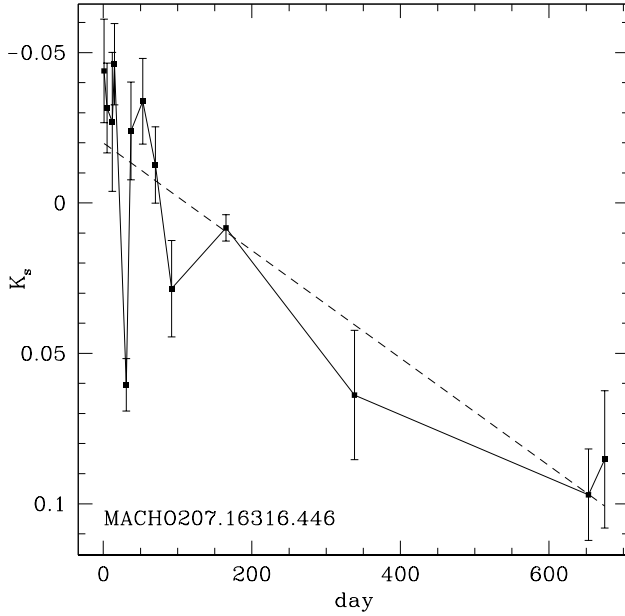


**Fig. 6.**  $K_s$  band variation of a QSO with respect to its mean magnitude as indicated in Table 2. Nightly averaged points are connected by a continuous line while a dashed line represents a linear fit through them. Error bars are the standard deviations from the mean. The slope of the line is  $1.8 \pm 0.4 \times 10^{-4}$  mag/day where day 0 corresponds to the first observation in the VMC data.

known QSOs to select a much tighter sample of candidates QSOs, a much greater fraction of which would be expected to be real QSOs when spectroscopically followed up.

As 75% of the known QSOs show a variation in the  $K_s$  band with a slope  $> 10^{-4}$  mag/day (Fig. 7) we expect 10 and 23 QSOs with this characteristic in tile LMC 6.6 and 8.8, respectively, among the magnitude, error and quality flag limited samples. These numbers have been confirmed by examining the light-curve variation of sources in these two tiles, for which all  $K_s$  epochs have been obtained by the VMC survey over a time range of 300 – 600 days.

To select objects with variability and colours like the known QSOs, we use criteria: photometric errors  $< 0.1$  mag, quality flags = 0 in  $YJK_s$ , a  $K_s$  slope of variation  $> 10^{-4}$  mag/day,  $Y < 19.32$  mag,  $J < 19.09$  mag and  $K_s < 18.04$  mag. We find a sample of 22 objects from tile LMC 8.8 of which 14, 7 and 1 located in region A, B and C respectively. This number is similar to the expected number of candidate QSOs derived earlier, i.e. 30 candidate QSOs are expected (Sect. 3.5.1) of which 75% ( $\sim 23$ ) show a variation in the  $K_s$  band with a slope  $> 10^{-4}$  mag/day. The same criteria applied to tile LMC 6.6 result in a sample of 26 objects, 15 and 11 in regions A and B respectively, while the large number of objects in region C reflects the contamination by reddened LMC variable stars. See Table 4 for details. This suggests that the combination of  $YJK_s$  colours and  $K_s$  variability selection is very effective in making a candidate QSO selection. The number of candidate QSOs would be larger if all sources of photometric class A are used.

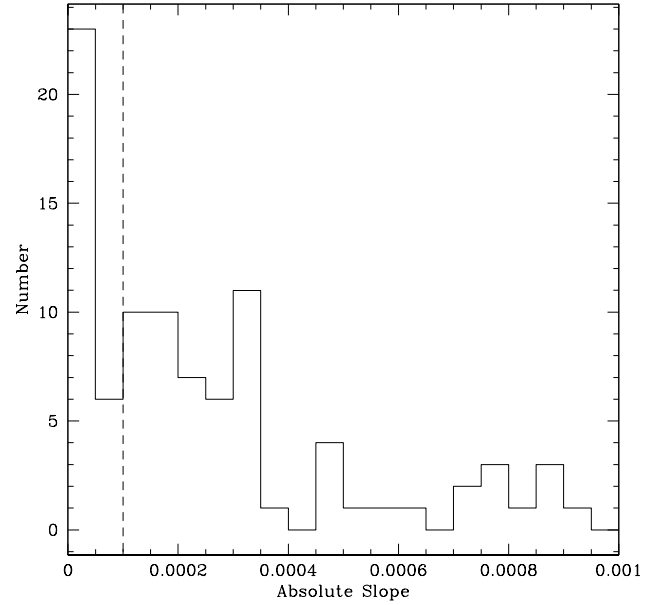


**Fig. 7.** Number of QSOs as a function of slope of variation in the  $K_s$  band. Each bin is  $0.5 \times 10^{-4}$  mag/day. A vertical dashed line is drawn at  $10^{-4}$  mag/day; 75% of the QSOs have slope larger than this value.

### 3.5.3. Identification of selected candidate QSOs

A detailed discussion of the true nature of the individual QSO candidates is beyond the primary aim of this study and it is postponed to when spectroscopic data becomes available. QSO contaminants are discussed in detail in the next section. However, counterparts to the 22 and 26 candidate QSOs in tile LMC 8.8 and 6.6, respectively, have been searched for in SIMBAD. One match, an X-ray sources was found in tile LMC 8.8. In tile 6.6 there are 3 X-ray sources and 1 young stellar object (YSO) in region A, and 1 X-ray source and 2 YSOs in region B. X-ray counterparts are usually found at a distance of up to  $1'$  while YSO counterparts are found at distances  $< 1''$ .

## 4. Discussion

We have established  $YJK_s$  colour-colour and  $K_s$  criteria to select candidate QSOs from VMC data. We now discuss the number and nature of objects which are not QSOs and which will also be selected by our criteria, to evaluate the degree of contamination of our sample of candidate QSOs that will not turn out to be QSOs.

### 4.1. QSO candidate contaminants

Photometric criteria for selecting QSOs often result in the misclassification of sources that show similar colours and magnitudes. The main contaminants in candidate QSO samples are normal galaxies, YSOs, PNe and evolved stars. Brown dwarfs have  $(Y - J) > 0.8$  mag while QSOs have  $(Y - J) < 0.8$  mag (Warren et al. 2007). The cool T-type dwarfs have also  $-1.5 < (J - K_s) < 0.5$  mag (Burningham et al. 2010) while

L-type dwarfs have  $(J - K_s) > 0.5$  mag (Knapp et al. 2004). Only the latter may be present in QSO regions BC (Fig. 2). In the next sections, the contribution by QSO candidate contaminants is discussed in more detail using the photometric study by Gruendl & Chu (2009), the spectroscopic studies by Kozłowski et al. (2012), Woods et al. (2011) and Kamath et al. (in prep.), and the recent study Kim et al. (2012) based on variability and photometric diagnostics.

#### 4.1.1. Gruendl & Chu (2009)

A statistically significant sample of QSO contaminants was assembled by Gruendl & Chu (2009) who analysed spectral energy distributions, from optical to mid-IR wavelengths, and mid-IR images from Spitzer in the central  $7^\circ \times 7^\circ$  area of the LMC. Their samples is: 949 definite and 126 probable background galaxies, 855 YSOs, 56 PNe, 159 diffuse sources, 117 evolved stars and 291 stars with IR excess have all been positionally matched with the present VMC data. We have excluded their lists of probable and possible YSOs since it is indicated that the first group may be background galaxies and the second group cannot be definitely classified.

The distribution of the matched sources in the colour-colour diagram is shown in Fig. 8. There are: 286 definite and 48 probable galaxies, 396 YSOs, 25 PNe, 123 diffuse sources, 44 evolved stars and 165 stars. The majority of these sources have counterparts within  $\sim 1''$  compared to an angular resolution of Spitzer of  $\sim 2''$  (Meixner et al. 2006). As expected, galaxies populate region A and B but most of them are located around the line separating them from the main locus of stars. This is also the preferred location of YSOs which extend to bluer colours and into region B. Most PNe are well confined in the region defined in Paper II while stars and diffuse sources occupy mostly regions C and D. A possible AGB star in the PNe region was found to be a PN by Miszalski et al. (2011a) and its colours are  $(Y - J) = 0.36$  and  $(J - K_s) = 2.16$  mag.

The sample of background galaxies by Gruendl & Chu (2009) contains a mixture of marginally resolved extended sources and extended sources with a point source nuclear region which were obtained from selection criteria tuned to find YSOs. They are therefore not representative of the background galaxy population in general. Among the sample of definite galaxies within the PN region Kamath et al. (in prep.) finds one QSO and one YSO out of three sources in common; the third one could not be classified due to low S/N spectral features. These findings suggest that the Gruendl & Chu's classification, which is based on photometric criteria, may not be reliable. Sources with a slope of variation in the  $K_s$  band  $> 10^{-4}$  mag/day represent a subset of the samples of QSO contaminants and their distribution in the colour-colour diagram is similar to that of the full samples (Fig. 8).

By considering only sources with photometric errors  $< 0.1$  mag and quality flags = 0 in each wave band, all YSOs are excluded (including the one above), only one star, a diffuse source and a PN remain in region B as well as two stars in region C while the number of background galaxies is also considerably reduced and confined within regions A and B, but for one source (Fig. 8). The main criterion responsible for the removal of sources is the requirement on the quality flags. In fact, the magnitudes of most sources were extracted following a de-blending process corresponding to flag = 16 (the confirmed QSO above has indeed this quality flag value in each

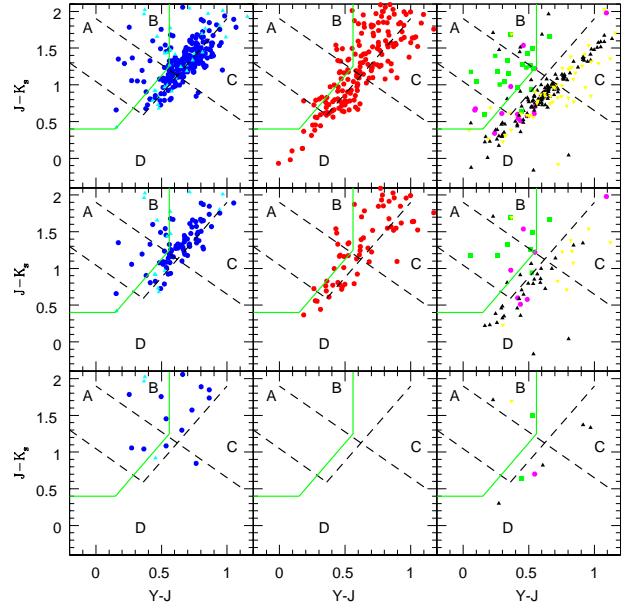


**Fig. 8.** Distribution of the Gruendl & Chu (2009) sources in the colour-colour diagram from present VMC data. (top row) All positionally matched sources. (middle row) Sources with a slope of variation in the  $K_s$  band  $> 10^{-4}$  mag/day. (bottom row) Sources with photometric errors  $< 0.1$  mag and quality flags = 0 in the  $Y$ ,  $J$  and  $K_s$  bands. (left column) Definite (blue circles) and probable (cyan triangles) background galaxies. (middle column) YSOs (red circles). (right column) PNe (green squares), diffuse sources (yellow reversed triangles), evolved stars (magenta circles) and other stars (black triangles). Lines are as in Fig. 2.

VMC wave band). Since the Gruendl & Chu's sample is unconfirmed, the remaining galaxies are either QSO contaminants or QSO candidates themselves while the influence of other sources is negligible. These galaxies are not previously known, all but one have a well defined star-like appearance in the VMC images and about half of them have a slope of variation in the  $K_s$  band  $> 10^{-4}$  mag/day.

#### 4.1.2. Kozłowski et al. (2012), Woods et al. (2011) and Kamath et al. (in prep.)

The spectroscopic investigation by Kozłowski et al. (2012) in the LMC produced not only a sample of 169 spectroscopically confirmed QSOs but also a sample of non-QSOs comprising: 112 YSOs, 17 PNe, 39 Be stars, 24 blue stars and 66 red stars. They also observed that 390 sources with  $I > 19$  mag are likely QSO candidates whose spectra are featureless and prevent a secure identification. Several non-QSOs were previously known. These objects were positionally matched to the VMC merged catalogue and counterparts were assigned to the nearest object within  $1''$ . This value is consistent with the mean distance to the QSOs derived in Sect. 2.3. The Kozłowski et al.'s non-QSO sample was complemented with the Spitzer spectroscopically confirmed LMC sources by Woods et al. (2011). These include: 90 AGB stars, 23 post-AGB stars, 7 PNe, 29 YSOs, 19 red supergiant stars and 7



background galaxies. Presently available VMC counterparts are at a distance of  $\sim 1''$ . A further non-QSO sample consisting of red-shifted normal and Seyfert galaxies, spectroscopically confirmed by Kamath et al. (in prep.) and covering sources behind both the LMC and SMC, was also positionally matched to the VMC data using the same criteria and included in the following discussion. The three studies considered here produce a large sample of non-QSOs. This sample is large enough to permit a reliable estimate of the contamination of QSO candidate samples by non-QSOs when the QSO candidates are selected on the basis of their position in the VMC colour-colour diagram and the slope of variation in the  $K_s$  band. It is not the aim of this investigation to discuss the completeness of the spectroscopic non-QSO sample.

The distribution of spectroscopically confirmed non-QSOs in the colour-colour diagram is shown in Fig. 9. There are 106 galaxies of which 7 are Seyferts, 41 YSOs, 9 PNe, 14 post-AGB stars, 11 blue stars (including Be stars) and 37 red stars (including AGB and red super giant stars). Ninety-four likely QSOs are also matched with the VMC data and shown in Fig. 9. Comparing Fig. 2 and 9, it seems that QSO candidates selected from the left side of the green line in regions A and B are unlikely to be contaminated by stars, galaxies or YSOs, but there will be a contamination by PNe. QSO candidates selected from region A but to the right of the green line will be contaminated by galaxies and YSOs. QSO candidates selected from region B but to the right of the green line will be contaminated by normal and Seyfert galaxies, YSOs and red stars. The sub-set of variable objects (with slope in the  $K_s$  band  $> 10^{-4}$  mag/day) weeds out contaminating red stars from regions B and C, and PNe from regions A and B while the distribution of galaxies and YSOs is unchanged. The distribution of objects with photometric errors  $< 0.1$  mag and quality flags = 0 results in a negligible number of galaxies and YSOs in regions B and C while none remain in region A. The Kozłowski et al.'s candidate QSOs populate the colour-colour diagram similarly to known QSOs (Fig. 2) and those that remain after applying variability, photometric uncertainty and quality flag criteria, are high confidence candidates also according to our study.

#### 4.1.3. Kim et al. (2012)

The MACHO database has been thoroughly mined for the identification of high confidence QSO candidates behind the LMC by Kim et al. (2012). Initially, using a method purely based on the QSO time variability, 2566 candidates were identified (Kim et al. 2011). With the additional information from observations at other wavelengths and the development of a model based on the diagnostics of known QSOs, 663 high confidence QSOs were later identified (Kim et al. 2012).

Figure 10 shows the distribution of the Kim et al.'s candidate samples positionally matched with the VMC data in the colour-colour diagram. There are 574 low confidence and 179 high confidence QSOs with a VMC counterpart within  $1.5''$  in the merged catalogue. The major point to notice is that low confidence QSOs are distributed mainly in region D while high confidence QSOs occupy mostly regions A and B. This is the case in general, for sources with a slope of variation in the  $K_s$  band  $> 10^{-4}$  mag/day and for sources with photometric errors  $< 0.1$  mag and quality flags = 0 in each wave band strongly supporting the criteria developed in this study.

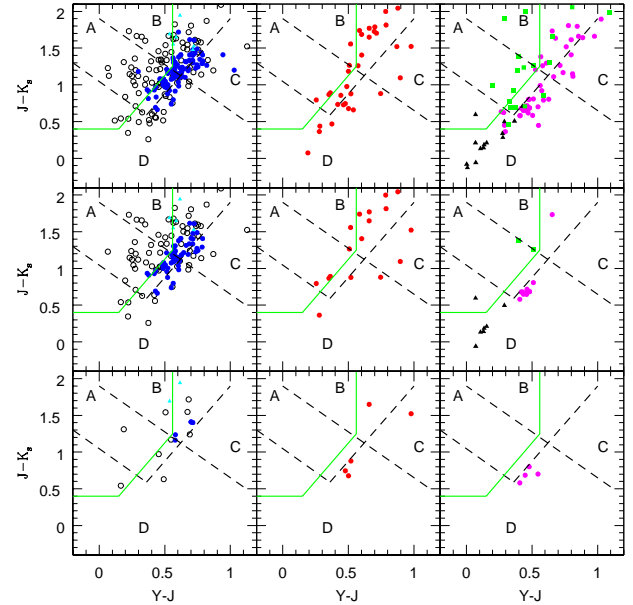


**Fig. 9.** Distribution of the Kozłowski et al. (2012), Woods et al. (2011) and Kamath et al. (in prep.) spectroscopically observed sources in the colour-colour diagram from present VMC data. (top row) All positionally matched sources. (middle row) Sources with a slope of variation in the  $K_s$  band  $> 10^{-4}$  mag/day. (bottom row) Sources with photometric errors  $< 0.1$  mag and quality flags = 0 in the  $Y$ ,  $J$  and  $K_s$  bands. (left column) Likely QSOs (black circles), normal (blue circles) and Seyfert galaxies (cyan triangles). (middle column) YSOs (red circles). (right column) PNe and post-AGB stars (green squares), red stars (magenta circles) and blue stars (black triangles). The lines are as in Fig. 2.

#### 4.2. QSO variability

While the optical variability of QSOs is well established (e.g. MacLeod et al. 2011) much less is known in the near-IR. The most recent investigation by Kozuma & Yamaoka (2012) addresses the properties of the ensemble variability of QSOs using two data points from the Two Micron All Sky Survey (2MASS; Skrutskie et al. 2006) and the DEep Near-Infrared Southern sky survey (DENIS; Epchtein et al. 1999) or the UKIRT Infrared Deep Sky Survey (UKIDSS; Lawrence et al. 2007). About 15 – 25% of the QSO emission in the  $K_s$  band is attributed to the accretion disc (Tomita et al. 2006) and the remaining to thermal radiation by dust in the AGN torus, heated by the disc (Barvainis 1987). The reason of variations in the  $K_s$  emission may be due to changes in the inner radius of the torus as a consequence of variations in the UV/optical flux from the AGN (Koshida et al. 2009, Kawaguchi & Mori 2011).

The best sampled near-IR QSO light-curves were obtained by the Multicolour Active Galactic Nuclei Monitoring (MAGNUM) programme on NGC 4151 and NGC 5548 (Yoshii, Kobayashi & Minezaki 2004; Koshida et al. 2009) or focused on 3C273 (Courvovsier et al. 1988) for a total of three sources. In the first study the  $K$  light-curves of the AGN nuclei, after subtracting the contribution from the host galaxy, show clear minima and maxima each over a time range of  $\sim 200$

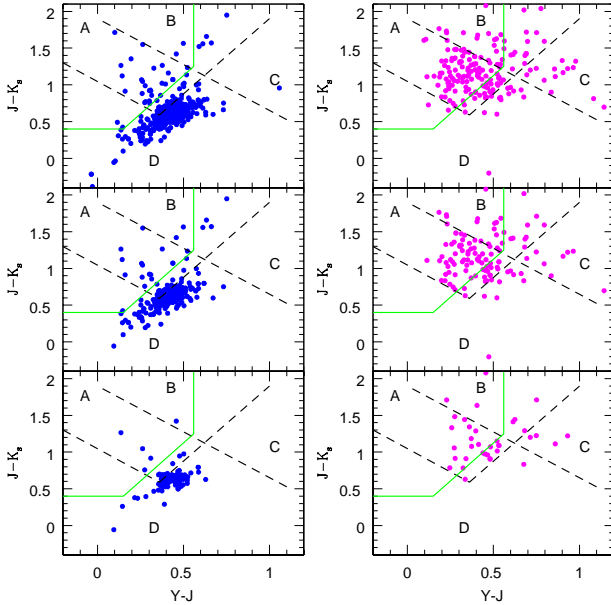


**Fig. 10.** Distribution of the Kim et al. (2012) sources in the colour-colour diagram from present VMC data. (top row) All positionally matched sources. (middle row) Sources with a slope of variation in the  $K_s$  band  $> 10^{-4}$  mag/day. (bottom row) Sources with photometric errors  $< 0.1$  mag and quality flags = 0 in the  $Y$ ,  $J$  and  $K_s$  bands. (left column) Low confidence QSOs (blue circles). (right column) High confidence QSOs (magenta circles). Lines are as in Fig. 2.

days. Overall the  $K$  variation is smoother than the variation in the  $V$  band which appears irregular and associated with rapid variations on time scales of several days. The luminous 3C273 source shows fast and structured flaring events also in the near-IR and only  $\sim 15$  days apart. Near-IR variations of QSO emission over a time range of up to twenty years but with a sparse sampling were also found by Neugebauer et al. (1989).

The VMC multi-epoch observations represent a considerable step forward in the study of QSO near-IR variations. The present sample shows both smooth trends, i.e. an increasing and decreasing brightness over a time range of 300–600 days, and structured events, i.e. broad (up to 100 days wide) and narrow (20–40 days wide) peaks, in agreement with previous studies. Despite the large number of QSO light-curves analysed in this study, there is no clear pattern of variation, but it is possible that similarities in the QSO light-curves occur across a time range of several years. In the future, when more QSO light-curves are available across a wide time range, we plan to construct empirical template light-curves from the combination of individual QSO light-curves with similar shape and structure functions (e.g. Hughes, Aller & Aller 1992). These can then be used to refine the search for QSOs and eventually to derive their redshift as in Dai et al. (2012). A theoretical interpretation of the VMC near-IR light-curves and structure functions may also provide further evidence for the mechanism responsible for the variations and contribute to studies of the structure and dynamics of the AGN (e.g. Wold, Brotherton & Shang 2007, Ovcharov et al. 2008).

#### 4.3. QSO numbers behind the Magellanic Clouds

Assuming that QSOs are homogeneously distributed across the surface of the Magellanic system we can use the number of VMC candidate QSOs derived in the previous sections to estimate the total number of QSOs detectable by the VMC survey. Using the magnitude limited sample in tile LMC 8.8, which is not affected by interstellar reddening and crowding since it is located in the outer disc of the galaxy, we derived that 22 objects are candidate QSOs. The VMC survey comprises of 110 tiles of which 68 in the LMC, 27 in the SMC, 13 in the Bridge and 2 in the Stream areas. The expected QSO population accessible to the VMC survey is thus of at least 1500 objects behind the LMC, 600 behind the SMC, 300 behind the Bridge and 50 behind the Stream areas. This means that  $\sim 85\%$  of the VMC accessible QSO population behind the Magellanic system is yet to be found. In addition, these numbers are conservative limits since they have originated from the application of magnitude, error, quality flag and variability restrictions.

## 5. Conclusions

The availability of large samples of QSOs across the Magellanic system is of fundamental importance as an astrometric reference source for investigations of the proper motion and for a study of the interstellar and intergalactic medium along the line of sight as well as to address the nature of the extra-galactic sources themselves. The search and characterisation of QSOs behind the Magellanic system is an on-going process as part of follow-up observations of large samples selected from optical light-curves and multi-wavelength photometry (Kozłowski et al. 2012). For a most efficient use of telescope time the determination of high confidence QSO samples is necessary (Kim et al. 2012).

We present criteria for selecting candidate QSOs based solely on the multi-epoch near-IR photometry from the VMC survey developed from the properties of 117 known QSOs observed behind the Magellanic system. Most known QSOs occupy two neighbouring regions of the  $(Y-J)$  vs.  $(J-K_s)$  diagram, one is dominated by QSOs with a star-like appearance and the other by QSOs with a galaxy-like appearance. The analysis of  $K_s$  multi-epochs shows that  $\sim 75\%$  of the QSOs have a slope of variation  $> 10^{-4}$  mag/day across a time range up to 600 days. The combination of  $YJ K_s$  colour-colour and  $K_s$  variability criteria, with appropriate data quality flags, can be used to define samples of candidate QSOs which should be relatively free of contamination by non-QSOs.

QSO candidates in LMC tile 6.6, including the 30 Doradus region, and 8.8, including the South Ecliptic Pole region, have been extracted from sources with photometric errors  $< 0.1$  mag and quality flags = 0 in each VMC wave band and brighter than 19.32, 19.09 and 18.04 mag in the  $Y$ ,  $J$  and  $K_s$  band, respectively. These magnitudes correspond to the faintest QSO in the sample by Kozłowski et al. (2012). Thirteen and 22 objects, respectively, satisfy the colour-colour and variability criteria. The selection of QSOs from the VMC data is in excellent agreement with the sample of high confidence QSOs by Kim et al. (2012).

The contamination by non-QSOs has been estimated using the photometric samples of YSOs, PNe, diffuse sources, evolved stars and other stars with IR excess, from Gruendl & Chu (2009) and spectroscopic samples from Kozłowski et al.



(2012), Woods et al. (2011) and Kamath et al. (in prep.). PNe represent the major source of contamination in the regions of the colour-colour diagram dominated by star-like QSOs while normal galaxies and YSOs are the major contaminants in the region dominated by galaxy-like QSOs. The sub-set of sources with a slope of variation in the  $K_s$  band  $> 10^{-4}$  mag/day is not influenced by PNe and red stars. The sub-set of sources with photometric errors  $< 0.1$  mag and quality flags = 0 in each VMC wave band is negligible. Since known QSOs may be de-blended and have quality flags = 16 the latter represents a reliable whilst not complete sample of candidates.

VMC magnitudes and  $K_s$  light-curves for known QSOs are provided in a table and in the appendix. The full sample of known QSOs comprises 332 QSOs from the literature and 28 newly confirmed QSOs by Kamath et al. (in prep.). VMC data on a fully observed tile in the outer LMC disc (8\_8) have been used to estimate the number of QSO candidates behind the entire system as covered by the VMC survey. This is of the order of 1500 behind the LMC, 600 behind the SMC, 300 behind the Bridge and 50 behind the Stream areas. Compared to the known number of QSOs in these regions  $\sim 85\%$  of the population is still missing. The VMC survey is the most sensitive near-IR survey of the Magellanic system to date providing for the first time near-IR counterparts to many QSOs. Spectroscopic observations of the candidates identified here will test the method and extend the selection to faint magnitudes exploiting the whole VMC range available.

*Acknowledgements.* MRC acknowledge support from the Alexander von Humboldt Foundation. This research has made use of the SIMBAD database operated at CDS, Strasbourg, France. We are grateful to ESO staff for scheduling and making the VMC observations, the Cambridge Astronomy Survey Unit and the Wide Field Astronomy Unit for providing us with the reduced data and catalogues. We thank M.I. Moretti and the anonymous referee for giving comments that improved the clarity of the paper.

## References

- Allcock, C., Allsman, R.A., Alves, D.R., et al., 2000, *ApJ*, 542, 281  
 Anguita, C., Patricio, L., & Pedreros, M.H., 2000, *AJ*, 120, 845  
 Barvainins, R., 1987, *ApJ*, 320, 537  
 Blanco, V.M., & Heathcote, S., 1986, *PASP*, 98, 635  
 Burningham, B., Pinfield, D.J., Lucas, P.W., et al., 2010, *MNRAS*, 406, 1885  
 Cardelli, J.A., Clayton, G.C., & Mathis, J.S., 1989, *ApJ*, 345, 245  
 Cioni, M.-R.L., Habing, H.J., & Israel, F.P., *A&A*, 358, L9  
 Cioni, M.-R.L., van der Marel, R.P., Loup, C., & Habing, H.J., 2000, *A&A*, 359, 601  
 Cioni, M.-R.L., Clementini, G., Girardi, L., et al., 2011, *A&A*, 527, A116, Paper I  
 Costa, E., Méndez, R.A., Pedreros, M.H., et al., 2011, *AJ*, 141, 136  
 Courvoisier, T.J.-L., Robson, E.I., Blecha, A., et al., *Nature*, 335, 330  
 Dai, D.-C., Starkman, G.D., Stojkovic, B., Stojkovic, D., & Weltman, A., 2012, *arXiv:1204.5191*  
 Dobrzycki, A., Groot, P.J., Macri, L.M., & Stanek, K.Z., 2002, *AJ*, 569, L15  
 Dobrzycki, A., Macri, L.M., Stanek, K.Z., & Groot, P.J., 2003a, *AJ*, 125, 1330  
 Dobrzycki, A., Stanek, K.Z., Macri, L.M., & Groot, P.J., 2003b, *AJ*, 126, 734  
 Dobrzycki, A., Eyer, L., Stanek, K.Z., & Macri, L.M., 2005, *A&A*, 442, 495  
 Emerson, J., & Sutherland, W., 2010, *The Messenger*, 139, 2  
 Epchtein, N., Deul, E., Derriere, S., et al., 1999, *A&A*, 349, 236  
 Eyer, L., 2002, *Acta Astron.*, 52, 241  
 Findlay, J.R., Sutherland, W.J., Venemans, B., et al., 2012, *MNRAS*, 419, 3354  
 Flesch, E., 2012, *PASA*, accepted  
 Geha, M., Allcock, C., Allsman, R.A., et al., 2003, *AJ*, 125, 1  
 Girardi, L., Groenewegen, M.A.T., Hatziminaglou, E., & da Costa L., 2005, *A&A*, 436, 895  
 Gruendl, R.A., & Chu, Y.-H., 2009, *ApJS*, 184, 172  
 Healey, S.E., Romani, R.W., Cotter, G., et al., 2008, *ApJS*, 175, 97  
 Haschke, R., Grebel, E., & Duffau, S., 2011, *AJ*, 141, 158

- Hony, S., Kemper, F., Woods, P.M., et al., 2011, *A&A*, 531, A137  
 Hook, I.M., McMahon, R.G., Boyle, B.J., & Irwin, M.J., 1994, *MNRAS*, 268, 305  
 Hughes, P.A., Aller, H.D., & Aller, M.F., 1992, *ApJ*, 396, 469  
 Irwin, M.J., Lewis, J., Hodgkin, S., et al., 2004, *SPIE*, 5493, 411  
 Kallivayalil, N., van der Marel, R.P., Alcock, C., et al., 2006, *ApJ*, 638, 772  
 Kawaguchi, T., & Mori, M., 2011, *ApJ*, 737, 105  
 Kerber, L.O., Girardi, L., Rubele, S., & Cioni, M.-R.L., 2009, *A&A*, 499, 697  
 Kim, D.-W., Protopapas, P., Byun, Y.-I., et al., 2011, *ApJ*, 735, 68  
 Kim, D.-W., Protopapas, P., Trichas, M., et al., 2012, *ApJ*, 747, 107  
 Knapp, G.R., Legget, S.K., Fan, X., et al., 2004, *AJ*, 127, 3553  
 Koshida, S., Yoshii, Y., Kobayashi, Y., et al., 2009, *ApJ*, 700, L109  
 Kouzuma, S., & Yamaoka, H., 2010, *A&A*, 509, A64  
 Kouzuma, S., & Yamaoka, H., 2012, *ApJ*, 747, 14  
 Kozłowski, S., Kochanek, C.S., 2009, *ApJ*, 701, 508  
 Kozłowski, S., Kochanek, C.S., & Udalski, A., 2011, *ApJ*, 194, 22  
 Kozłowski, S., Kochanek, C.S., Jacyszyn, A.M., et al., 2012, *ApJ*, 746, 27  
 Lawrence, A., Warren, S.J., Almaini, O., et al., 2007, *MNRAS*, 379, 1599  
 MacLeod, Brooks, K., Ivezić, Ž., et al., 2011, *ApJ*, 728, A26  
 Maddox, N., & Hewett, P.C., 2006, *MNRAS*, 367, 717  
 Maddox, N., Hewett, P.C., Warren, S.J., & Croom, S.M., 2008, *MNRAS*, 386, 1605  
 Maddox, N., Hewett, P.C., Péroux, C., Nestor, D.B., & Wisotzki, L., 2012, *MNRAS*, accepted  
 Meixner, M., Gordon, K., Indebetouw, R., et al., 2006, *AJ*, 132, 2268  
 Miszalski, B., Napiwotzki, R., Cioni, M.-R.L., & Nie, J., 2011a, *A&A*, 529, A77  
 Miszalski, B., Napiwotzki, R., Cioni, M.-R.L., et al., 2011b, *A&A*, 531, A157, Paper II  
 Mortlock, D., Warren, S.J., Venemans, B.P., et al., 2011, *Nature*, 474, 616  
 Mortlock, D., Patel, M., Warren, S.J., et al., 2012, *MNRAS*, 419, 390  
 Neugebauer, G., Soifer, B.T., Matthews, K., & Elias, J.H., 1989, *AJ*, 97, 957  
 Ovcharov, E.P., Nedialkov, P.L., Valcheva, A.T., et al., 2008, *MNRAS*, 386, 819  
 Perlman, E.S., Padovani, P., Giommi, P., et al., 1998, *AJ*, 115, 1253  
 Pedreros, M.H., Anguita, C., & Maza, J., 2002, *AJ*, 123, 1971  
 Polletta, M., Tajer, M., Maraschi, L., et al., 2007, *ApJ*, 663, 81  
 Redfield, S., Gibson, B.K., Thom, C., et al., 2006, *AAO Newsletter*, 110, 9  
 Schlegel, D.J., Finkbeiner, D.P., & Davis, M., 1998, *ApJ*, 500, 525  
 Schmidt, M., 1968, *AJ*, 151, 393  
 Schneider, D.P., Richards, G.T., Hall, P.B., et al., 2010, *AJ*, 139, 2360  
 Shanks, T., Georgantopoulos, I., Stewart, G.C., et al., 1991, *Nature*, 353, 315  
 Stern, D., Eisenhardt, P., Gorjian, V., et al., 2005, *ApJ*, 631, 163  
 Skrutskie, M.F., Cutri, R.M., Stiening, R., et al., 2006, *AJ*, 131, 1163  
 Tinney, C.G., Da Costa, G.S., & Zinnecker, H., 1997, *MNRAS*, 285, 111  
 Tinney, C.G., 1999, *MNRAS*, 303, 565  
 Tomita, H., Yoshii, Y., Kobayashi, Y., et al., 2006, *ApJ*, 652, L13  
 Udalski, A., Szymański, M., Kałużny, J., et al., 1992, *Acta Astron.*, 49, 201  
 Vanden Berk, D.E., Richards, G.T., Bauer, A., et al., 2001, *AJ*, 122, 549  
 van Loon, J.Th., Smith, K.T., McDonald, I., et al., 2009, *MNRAS*, 399, 195  
 Véron-Cetty, M.-P., & Véron, P., 2010, *A&A*, 518, A10  
 Warren, S.J., Hewett, P.C., & Foltz, C.B., 2000, *MNRAS*, 312, 827  
 Warren, S.J., Mortlock, D.J., Legget, S.K., et al., 2007, *MNRAS*, 381, 1400  
 Wold, M., Brotherton, M.S., & Shang, Z., 2007, *MNRAS*, 375, 989  
 Woods, P.M., Oliveira, J.M., Kemper, F., et al., 2011, *MNRAS*, 411, 1597  
 Yoshii, Y., Kobayashi, Y., & Minezaki, T., 2004, *Astron. Nachr.*, 6, 540  
 Zaritsky, D., Harris, J., Thompson, I.B., & Grebel, E.K., 2004, *AJ*, 128, 1606

## Appendix A: $K_s$ band light-curves of known QSOs

Figure A.1 shows the  $K_s$  band light-curves of known QSOs in the presently available VMC data (VSA data release VMCv20120126) where single epoch data are included for completeness.

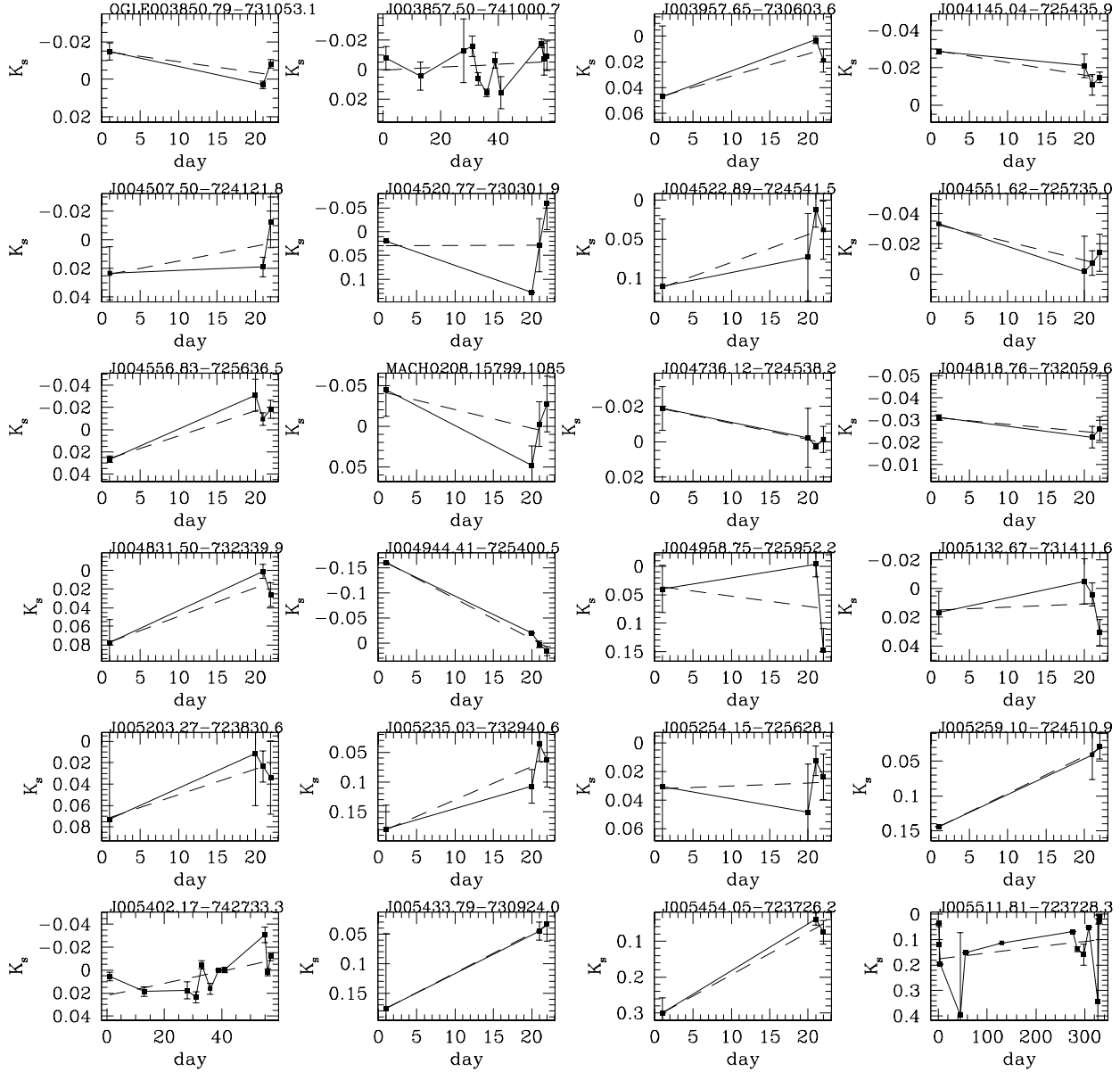


**Fig. A.1.**  $K_s$  band light-curves of known QSOs with respect to their mean magnitude. From top to bottom and left to right they follow the order in Table 2. Points represent the simple average of observations obtained within the same night/epoch and error bars correspond to the error of the mean. A continuous line connects the data points while a dashed line represents a linear fit through them. Day 0 corresponds to the first observation in the VMC data. Single epoch data are included for completeness.

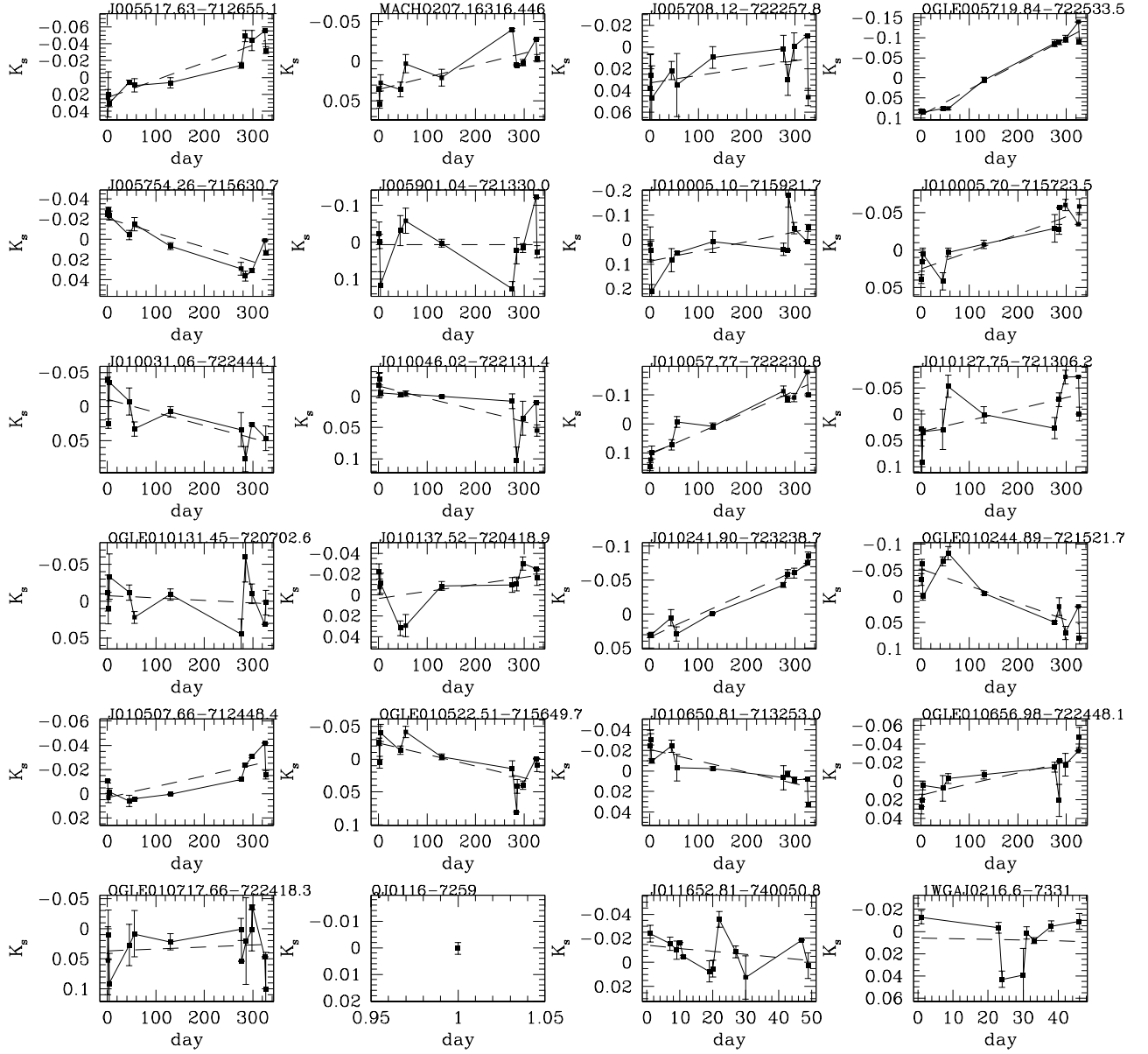


Fig. A.1. continued.

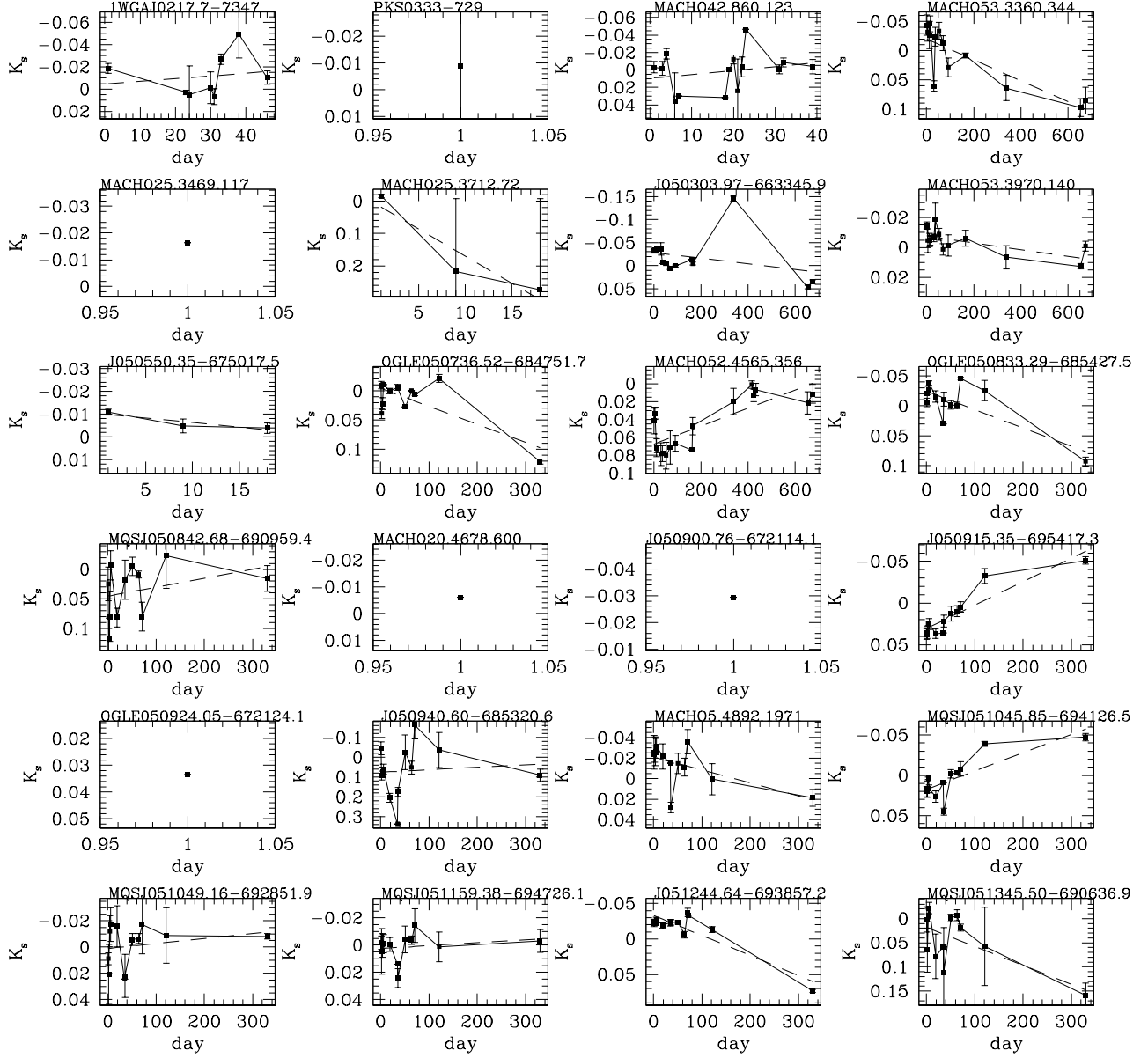


Fig. A.1. continued.

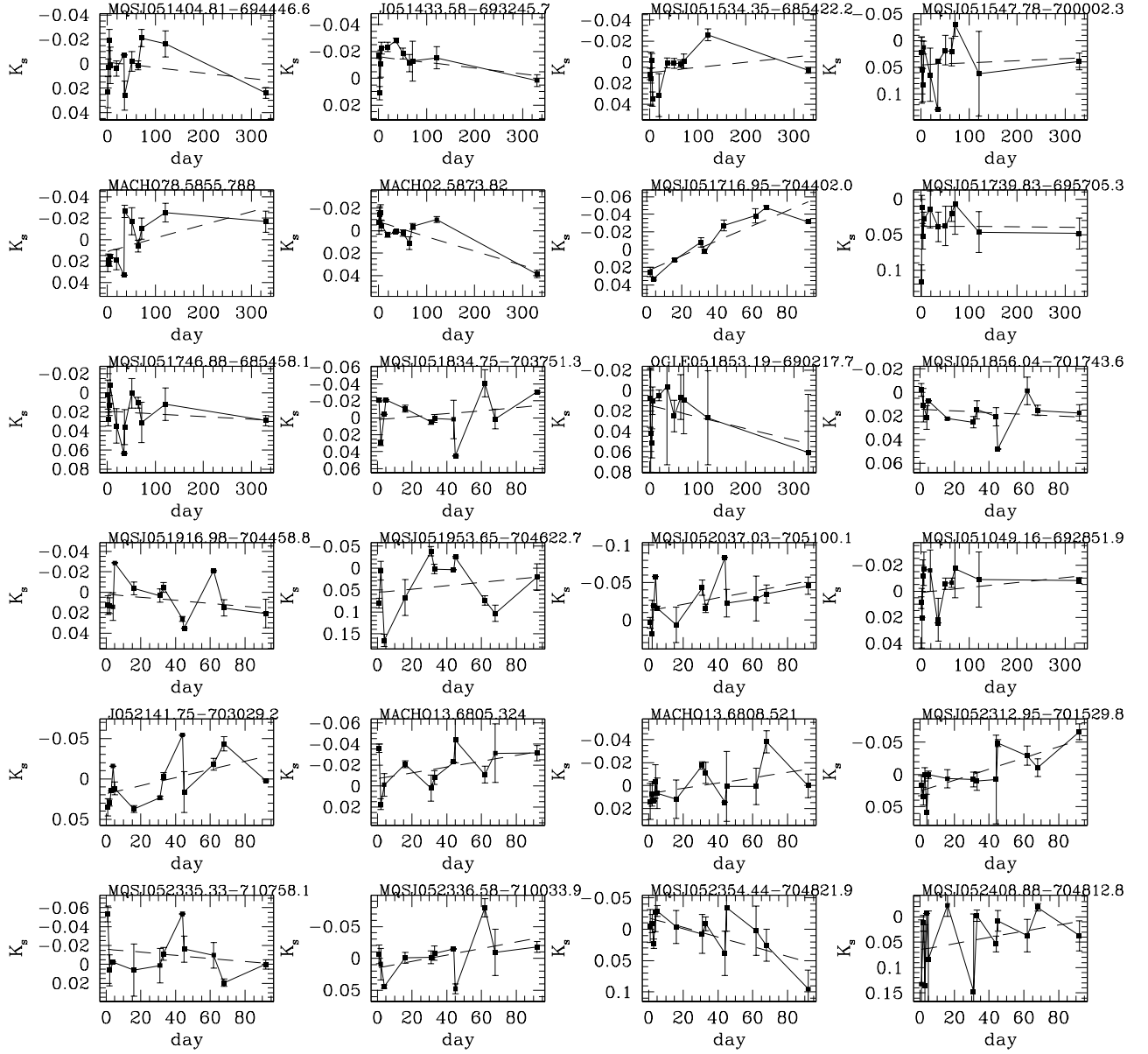


Fig. A.1. continued.

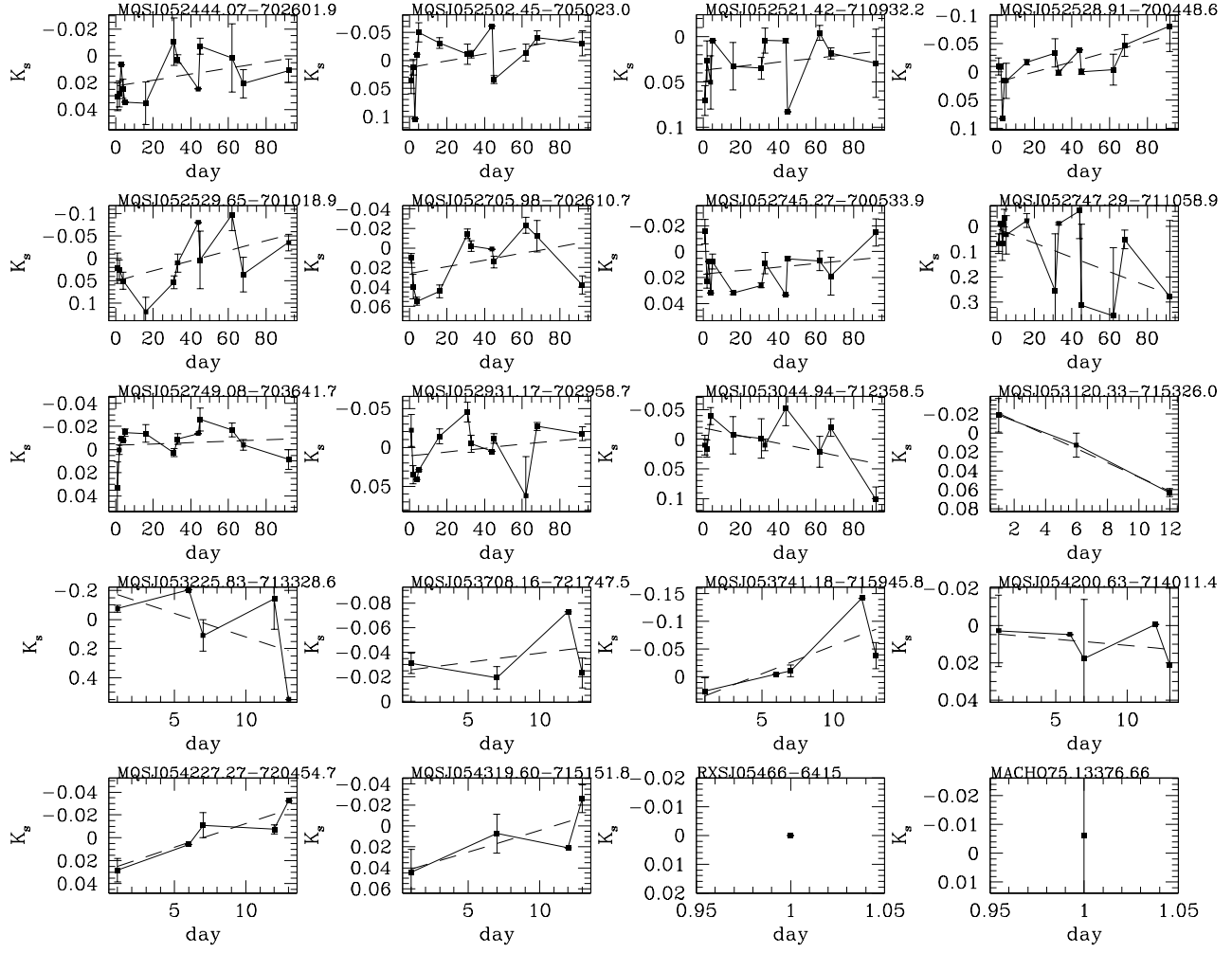


Fig. A.1. continued.